Research

Modelling of Radionuclide Transport by Groundwater Motion in Fractured Bedrock for Performance Assessment Purposes

Anders Wörman
Joel Geier
Shulan Xu

October 2003

SKi

SKI perspective

Background

The Swedish site investigation programme is ongoing and is rapidly producing site specific data that will be included in SKB's site descriptive models, preliminary safety evaluations and in the final safety assessments SR-Can and SR-Site. To be prepared for the review of these reports, SKI will need to perform some independent modelling as regards groundwater flow and radionuclide transport, using a selection of the available site specific data.

The purpose of this study is to develop a performance assessment (PA) model for analyses of radionuclide transport in the geosphere that accounts for the effect of heterogeneities of hydrological as well as geochemical rock properties. This is accomplished by coupling of sub-models for water flow (the discrete-fracture network model developed for SKI by Joel Geier, Geier 2004) and solute transport (developed by Xu et al, 2001 and Wörman et al., 2003). Moreover, measured geochemical data from Äspö Hard Rock Laboratory in Sweden is used to exemplify how the discrete-fracture and the solute transport models are coupled. The coupled model also enables an assessment of whether a process, that is important in the small scale (time or space), is important also on the larger geosphere scale.

Relevance for SKI

The work presented in this report is a step forward in developing a coupled groundwater flow and radionuclide transport model and as such is an important part of SKI's work in PA modelling.

The proposed approach includes numerical simulations of the three-dimensional fluid flow in a discrete feature network and a one-dimensional analytical solution of heterogeneous (random) mass transfer through the series of fractures. This method leads to a mathematically simple coupling of the solute transport with the three-dimensional flow problem as well as rapid computations that are suitable for future risk assessments and performance assessments.

Results

This study has successfully coupled a three-dimensional flow model and a one-dimensional mass transfer model, thereby creating an integrated model suitable for risk assessments and performance assessments.

Preliminary analyses performed with this integrated model indicate that regional/global variability in flow velocity and fracture aperture dominates over the local-scale variability as regards the effect on solute transport. However, site-specific data on both a fracture (local) scale and regional scale is required to reach a definite conclusion regarding the relative importance of local- and regional-scale variability.

It is also shown that the effect of heterogeneous rock properties on radionuclide transport in rock fractures increases markedly with decreasing fracture aperture and the co-varying advection velocity. It is concluded that the effect of variability in bedrock properties on the larger network-scale may be much larger that on the local scale. This may have a great importance for implementation in for instance risk assessments.

Future work

Future activities will be to take this work forward within the framework of the SKI performance assessment group that meets regularly two times per year to discuss ideas and present results from various projects dealing with issues relevant for PA modelling.

Project information

SKI project manager: Eva Simic
Project Identification Number: 14.9-011347/01288

Modelling of Radionuclide Transport by Groundwater Motion in Fractured Bedrock for Performance Assessment Purposes

Anders Wörman[1]
Joel Geier[2]
Shulan Xu[3]

[1]Department of Biometry and Engineering
Swedish University of Agricultural Sciences
Box 7013
SE-750 07 Uppsala, Sweden

[2]Clearwater Hardrock Consulting
14505 Corvallis Rd
Monmouth
OREGON 97361-9603, USA

[3]Swedish Radiation Protection Authority, SSI
SE-171 16 Stockholm

October 2003

Contents

Summary

Field data of physical properties in heterogeneous crystalline bedrock, like fracture zones, fracture connectivity, matrix porosity and fracture aperture, is associated with uncertainty that can have a significant impact on the analysis of solute transport in fractured rock. The purpose of this study is to develop a performance assessment (PA) model for analyses of radionuclide transport in the geosphere, in which the model takes into account both the effect of heterogeneities of hydrological and geochemical rock properties.

By using a travel time description of radionuclide transport in rock fractures, we decompose the transport problem into a one-dimensional mass transfer problem along a distribution of transport pathways and a multi-dimensional flow problem in the fractured bedrock. The hydraulic/flow problem is solved based on a statistical discrete-fracture model (DFM) that represents the network of fractures around the repository and in the surrounding geosphere. A Monte Carlo technique reflects the fact that the representation of the fracture network is uncertain.

If the flow residence time PDF exhibits multiple peaks or in another way shows a more erratic hydraulic response on the network scale, the three-dimensional travel time approach is superior to a one-dimensional transport modeling. Examples taken from SITE 94, a study performed by the Swedish Nuclear Power Inspectorate, showed that such cases can be found in safety assessments based on site data.

The solute transport is formulated based on partial, differential equations and perturbations (random spatial variability in bedrock properties) are introduced in the coefficients to reflect an uncertainty of the exact appearance of the bedrock associated with the discrete data collection. The combined approach for water flow and solute transport, thereby, recognises an uncertainty in our knowledge in both 1) bedrock properties along individual pathways and 2) the distribution of pathways.

Solutions to the central temporal moments of the residence time probability density function (PDF) for solutes in both one and three dimensions are derived in closed form for a solute Dirac pulse. The solutions are based on a model that takes into account advection along the network of fracture planes, diffusion into the rock matrix and sorption kinetics in the rock matrix. The most relevant rock properties including fracture aperture and several matrix properties as well as flow velocity are assumed to be spatially random along transport pathways.

The auto-covariance function representing the spatial variability in a rock property is also separated in terms of local variations, within individual fractures, and regional/global variations in a network of fractures. Analyses indicate that the regional/global variation probably dominates over the local variation due to the longer correlation lengths. This may have implications for planning of data collection, in which it is likely that one should pay more attention to the large-scale variations in bedrock properties. However, site-specific data (e.g. on the variance) is needed also on the single fracture-scale to be able to draw general conclusion on this issue.

Furthermore, measured geochemical data from Äspö Hard Rock Laboratory in Sweden is used to exemplify how the discrete-fracture and the solute transport models are coupled. Experimental studies based on rock samples taken at Äspö Hard Rock Laboratory, reveal that crystalline bedrock can possess a marked heterogeneity of various physical and geochemical properties even on a fracture-scale. By inserting measurement values in the solutions we can conclude that the heterogeneity of the rock properties in single fractures contributes to increasing significantly both the variance and the skewness of the residence time probability density function for a pulse travelling in a fracture. The Äspö-data suggests that the bias introduced in the variance of the expected value of the residence time PDF for radionuclides by neglecting the heterogeneity of the rock properties is very large for fractures thinner than a few tenths of a millimetre. This bias would be even larger if the large-scale variation in bedrock properties on the network-scale was also accounted for.

Sammanfattning

Fältdata över fysikaliska storheter i heterogent kristallint berg, som sprickzoner, spricknätverkan, matrisporositet, och sprickaperturer, uppvisar stora osäkerheter vilka kan ha en väsentlig betydelse för analyser av radionuklidtransport i sprickigt berg. Syftet med projektet som beskrivs i denna rapport var att utveckla en modell över radionuklidtransport i sprickigt berg som tar hänsyn till effekterna av heterogenitet i hydrologiska och geokemiska egenskaper i berget. Modellen skall även vara användbar i säkerhetsanalyser över slutförvaret av radioaktivt avfall med hänsyn till beräkningstid och dataunderlag.

Genom att utgå från en beskrivning av uppehållstider (residenstider) för vattnets tredimensionella rörelse längs olika flödesbanor, kan ämnestransporten analyseras i en dimension längs dessa banor. Även om flödesberäkningen kräver komplicerade och arbetskrävande numeriska operationer ger denna metod väsentliga arbetsbesparingar både i beräkningsarbetet och i hantering av data. Lösningen till flödesproblemet baseras på en statistisk representation av diskreta (enskild) sprickor i ett nätverk kring slutförvaret och i den omgivande geosfären. Monte Carlo (statistiska) dator simuleringar reflekterar det faktum att de hydrologiska parametrarna är osäkra.

Om residenstidsfördelningen för flödet uppvisar flera toppar, på grund av flera dominerande flödesvägar i nätverket av sprickor, så är den tredimensionella (uppehållstids-) beskrivningen väsentligt bättre än en endimensionell modellering. Eventuella brister i modellbeskrivningen gäller både koncentrationstoppar och varaktigheten i ett spridningsförlopp. Exempel som utvecklats från underlag i SITE 94, undersökningen som genomfördes av Statens kärnkraftsinspektion, visar att det mycket väl kan förekomma sådana flera flödesvägar i säkerhetsanalyser tillämpade på det svenska urberget.

Den lösta ämnestransporten formuleras med hjälp av partiella differentialekvationer. Perturbationer (statistiska störningar) införs i koefficienterna för att representera osäkerheterna den rumsliga variationen i bergets egenskaper som uppkommer på grund av den punktvisa datainsamlingen. Det kombinerade angreppssättet för flöde och löst ämnestransport tar därmed hänsyn till vår bristande kunskap om både 1) berggrundens egenskaper längs enskilda transportvägar och 2) fördelningen av transportvägar.

I rapporten härleds lösningar i sluten form till de centrala temporala momenten av täthetsfunktionen för uppehållstiderna för lösta ämnen i både en och tre dimensioner. Lösningarna tar hänsyn till advektion längs nätverket av sprickplan, diffusion och sorptionskinetik i bergmatrisen. De flesta relevanta storheterna, inklusive sprickapertur, en rad storheter för bergmatrisen samt flödeshastigheten antas vara rumsligt slumpmässiga längs transportbanorna.

Auto-kovariansfunktionen, som representerar den rumsliga variabiliteten i bergets egenskaper, är separerad i form av en lokal variation, inom enskilda sprickor, och en regional/global variation i spricknätverket. Analyser indikerar att den regionala (storskaliga) variationen förmodligen dominerar lösningen över de lokala variationerna på grund av längre korrelationslängder. Detta kan ha betydelse för planering av provtagningar genom att det förmodligen är viktigare att kunna beskriva de storskaliga variationerna i bergets egenskaper. Dock är det viktigt att ha platsspecifika data (t.ex. över varians) för att kunna dra definitiva slutsatser kring denna fråga.

Dessutom används geokemiska data från Äspö berglaboratorium för att exemplifiera hur den diskreta nätverksmodellen och modellen över den lösta ämnestransporten kan kopplas. Experimentella undersökningar baserat på prover från Äspö berglaboratorium visar att kristallint berg kan ha markanta variationer i olika fysikaliska och geokemiska egenskaper till och med i enskilda sprickor. Genom att sätta in mätvärden i de analytiska lösningarna kan man konstatera att heterogeniteterna i bergets egenskaper i enskilda sprickor bidrar väsentligt till att öka både varians och skevhet i uppehållstidsfördelningen för en ämnespuls i sprickan. Äspödatat indikerar att felet som uppkommer i variansen i den väntevärdesbildade uppehållstidsfördelningen för radionuklider genom att försumma heterogenitet i bergets egenskaper är mycket stort för sprickor som är tunnare än några tiondels millimeter. Felet skulle bli ännu större om man även tog hänsyn till de mer storskaliga variationerna i berget.

1. Introduction

Performance assessment of the Swedish final disposal for spent nuclear fuel involves modelling of possible leakage of radionuclides from a damaged canister in the deep bedrock repository. One of the important issues for the performance assessment is how data uncertainty and uncertainty due to spatial variability in rock properties can be addressed in the modelling and data acquisition.

Transport of solutes in fractured rock is affected by advection in conducting fractures and matrix diffusion as well as sorption onto the solid matrix. Various models have been developed to describe solute transport in fractures subjected to matrix diffusion and sorption (e.g. Neretnieks 1980, Grisak and Pickens, 1980 and Wels et al. 1994).

Most models describing radionuclide transport in fractured bedrocks do not include the effect of heterogeneity in rock properties and sorption kinetics on solute mass transfer. However, the impact of aperture heterogeneity in an individual fracture on solute transport has been described numerically using particle-tracking simulations (e.g. Moreno et al., 1988). Cvetkovic et al. (1999) analysed the effect of heterogeneous aperture and matrix diffusion on solute transport in a single fracture in terms of two spatially random parameters using a Monte Carlo technique. Recently, Painter and Cvetkovic (2001) extended their analysis of heterogeneous aperture and matrix diffusion to solute transport on a fracture network scale but without account taken to the effect of aperture heterogeneity on the flow distribution.

The purpose of this study is to develop a performance assessment (PA) model for analyses of radionuclide transport in the geosphere, in which the model takes into account both the effect of heterogeneous rock properties on mass transfer and aperture heterogeneity on the flow distribution. An alternative to achieve this objective is to use Monte Carlo simulations based on 3-D models that account for both hydraulics and solute mass transfer. However, such an approach would need unrealistically long computing time and this prohibits systematic investigations. A particularly fast method is required if the transport model is included in a risk framework with a large sequence or tree structure of models representing an entire pathway from the fuel rods to individual humans and possible evolution scenarios.

By using a travel time description of radionuclide transport in rock fractures, we decompose the transport problem into a one-dimensional mass transfer problem and a multi-dimensional flow problem. The proposed approach includes numerical simulations of the three dimensional fluid flow in a discrete feature network and a one-dimensional analytical solution of heterogeneous (random) mass transfer through the series of fractures. Hence, the de-coupling significantly reduces computational requirements both because the randomness of the flow and the solute transport are decoupled and because the solute transport is one-dimensional. The latter simplification implies important possibilities to solve the solute mass transport in certain closed-forms that will be discussed in this report. Furthermore, this method leads to a mathematically simple coupling of the solute transport with the three-dimensional flow problem and rapid computations that are suitable for future risk or performance assessments.

The hydraulic/flow problem is solved based on a statistical discrete-fracture network model that represents the system of fractures around the repository. This sub-model is described in more detail in another SKI-report (Geier, 2003) and will not be described in full detail here. The main purpose of this report is to demonstrate how the sub-models for water flow and solute transport are coupled and, particularly, to give examples on the use of field data in site specific investigations. A particular focus is on the stochastic solution techniques applied to the solute transport. Further, measured field data from Äspö Hard Rock Laboratory is used to exemplify how the discrete-fracture and the solute transport models are coupled.

A main problem is how to account for heterogeneity in rock properties. Recent experimental studies reveal that crystalline bedrock can possess a marked heterogeneity of various physical and geochemical properties (Hakami and Barton, 1990; Siitari-Kauppi et al., 1997; Xu and Wörman, 1998; Johansson, 2000) that potentially may have a certain impact on the transport of radionuclides in fractured bedrock. In addition, current field investigation techniques provide only fragmentary information of the properties of the geosphere. This is a basic motivation for treating flows of water and solute elements in groundwaters by means of stochastic models (Gelhar et al. 1974; Dagan, 1989; Gutjhar et al. 1978; Gelhar and Axness, 1983). The macro-dispersion in fractured bedrock has been studied, particularly using stochastic discrete fracture networks (e.g. Andersson and

Dverstorp, 1987; Dverstorp et al., 1992) and stochastic continuum models for the groundwater flow (e.g. Neuman, 1987; Schwartz and Smith, 1988).

The methodology proposed here is based on a combination of two stochastic techniques. The fluid flow is treated using discrete fracture models (DFM) with a Monte Carlo technique to reflect the fact that the representation of the fracture network is uncertain. The solute transport is solved using stochastic continuum according to Xu et al. (2001) and Wörman et al. (2003), which implies that perturbations are introduced in the coefficients of the partial differential equation system describing the transport processes. In this connection, we recognise a random spatial variability in bedrock properties along a specific pathway but also a distribution of equally probable pathways. This approach is adopted to reflect our uncertainty of the bedrock associated with the discrete data collection.

If we were able to estimate the exact distribution of parameter values from a large number of samples it would be relevant to perform a deterministic analysis of the transport. The stochastic analysis is based on the idea that we know only certain point values of the property fields and use this information to estimate intermediate values. Consequently, there are two important problems (at least) related to the spatial variability of rock properties, effects of the actual (real) spatial parameter variability along the pathway (if we knew the parameter set up exactly) and effects due to the uncertainty in our knowledge of the heterogeneous rock properties. The first problem can be analysed based on a deterministic description of the parameter variability, whereas the second problem requires a stochastic approach. In this study we outline the implications of the two approaches. Further we show how the stochastic approach can be supported by geo-statistical data obtained from rock samples.

The report contains a comparison between a 1-D transport model and a 3-D formulation of solute transport using the travel time approach and site-specific data. A sensitivity analysis shows the effect of the information neglected in the 1-D model/analysis. We also demonstrate the combined effect of the uncertainty due to the spatial variability of water flow and solute mass transfer using the proposed model. The data used in the simulations are collected at Äspö Hardrock Laboratory. The analyses are based on the statistics of aperture and rock properties for a single fracture obtained from

experimental data and statistics of aperture of the network obtained from geological mapping.

The study also comprises a study of the longitudinal dispersion in the discrete feature network. A relationship between longitudinal dispersion coefficient and Peclet number is studied in single fractures by using numerical particle-tracking experiments, in which the effect of microscopic dispersion due to shear dispersion and molecular dispersion is taken into account.

2. Theoretical background

In this chapter we present two methods that are used in combination to analyse solute transport in fractured rock; one is the travel time approach (section 2.1) and the other is the one-dimensional stochastic continuum model (section 2.7). The stochastic mass transfer model used in the travel time approach is stated in section 2.2, in which the model takes into account both deterministic (real) variability of rock properties and effects due to the uncertainty in our knowledge of the heterogeneous rock properties. Sections 2.3 and 2.5 discuss, respectively, the effects of real variability of rock properties along the transport path and effects of our uncertainty of rock properties on transport. In section 2.5, we present the details of derivations of analytical mean value solutions of stochastic mass transfer equations by using a small perturbation approach combined with spectral analysis. The solutions are extended to a network scale in section 2.6.

2.1 3-D flow and travel time description of solute transport

The three-dimensional analysis of the mass flow can be performed by studying the change of the solute mass in water parcels travelling along a large number of trajectory paths. In a Lagrangian framework, or a travel time description, the transport problem is thus decomposed into a two-dimensional flow problem, in which the trajectory paths of inert water parcels are determined, and a one-dimensional solute transport problem in which the mass-transfer between the parcels and rock matrix is determined. Here, we can obtain the expected probability density function (PDF) of the residence time for water in the whole distribution of trajectories in the fracture network as (Dagan, 1989; Rodriguez-Iturbe and Rinaldo, 1997)

$$< f(t, \tau) >= \int_0^\infty f(t, \tau) g(\tau) d\tau \qquad (1)$$

in which $g(\tau)$ is the travel time probability density function (PDF) for a large number of inert water parcels arriving at a certain control section for the whole distribution of trajectories in fracture network, τ is the residence time of an inert water parcel traveling

along one of the trajectory paths, and f(t, τ) is the residence time PDF of solute mass in the water parcel, where $f(t, \tau) = c(t, \tau)/m_0$, m_0 is the zeroth moment of c (area under the curve c(t)), c is the concentration of solute per unit volume of fracture water [kg/ m^3] and t is the time [s]. In the following sections we describe how f(t, τ) and g(τ) can be obtained.

An estimate of the residence-time PDF, g(τ), of inert water parcels travelling through fractured bedrock, from damaged canisters to discharge locations, can be obtained from the 3-D groundwater flow model by advective-dispersive particle tracking in the flow field of the heterogeneous rock (see section 4). Information from such models can also be used to interpret hydrological parameters for use in one-dimensional continuum models of radionuclide transport. In such a case, the relevant parameters are Darcy velocity, effective longitudinal dispersion coefficient, flow porosity and flow-wetted surface.

Two contrasting methods for representing the hydrologic character of fractured bedrock are the discrete-feature and continuum methods. In the discrete-feature (DF) method, which is applied here, the bedrock is represented as a 3-D network of transmissive features representing individual fractures, described in terms of statistical distributions of fracture parameters such as size, orientation and aperture, and larger-scale transmissive structures such as fracture zones, which may be represented either deterministically or statistically.

In continuum models, the detailed structure of the represented rock is generally not taken into account, and an assumption must be introduced that the network of fractures within the bedrock are sufficiently well-connected to behave as an equivalent porous medium on the scale of the blocks in the continuum model. This assumption cannot always be demonstrated to hold in sparsely fractured rock (Long, 1984). Even when a fracture network behaves effectively as a continuum on a block scale, estimates of hydraulic conductivity from borehole measurements may be poorly correlated to block-scale properties, since borehole tests preferentially sample a subset of the fractures within a given block (Geier et al., 1992).

In the present study, the DF method is used to develop examples for illustrating the travel-time approach, because of its stronger physical basis and capacity for utilisation of structural geologic information.

2.2 Theory for one-dimensional solute transport

Transport of radionuclides in fractured rock is affected by advection and diffusion in conducting fractures as well as diffusion into micro-fissures of the rock matrix (matrix diffusion) and sorption onto the solid matrix. The relative importance of longitudinal dispersion (or diffusion) in the fracture and matrix diffusion is governed by two Peclet numbers, $(uh)/E$ and $(uZ)/(\varepsilon D_p)$, where D_p is the pore diffusivity [m^2/s], ε is the total porosity of rock matrix, E is the longitudinal dispersion coefficient [m^2/s], h is the fracture aperture [m], u is the advection velocity in the fracture [m/s] and Z is the matrix depth to which matrix diffusion can occur [m]. Based on the coefficient of variation of solute residence times in a single fracture, $CV(t)$ (following the approach of Xu and Wörman, 1999), we find that matrix diffusion dominates the effect on $CV(t)$ if their product, $(Zhu^2)/(E\varepsilon D_p)$, is sufficiently large. Consistently, the effect of longitudinal diffusion has been omitted in a number of studies on radionuclide migration in an individual fracture (Neretnieks, 1980; Cvetkovic et al., 1999).

If radioactive decay and surface diffusion are disregarded, a kinematic formulation for the solute mass transport in one dimension can be given as (Xu and Wörman, 1999)

$$\frac{\partial \tilde{c}}{\partial t} + \tilde{u}\frac{\partial \tilde{c}}{\partial x} - 2\frac{\tilde{\varepsilon}_t \tilde{D}_p}{\tilde{h}}\frac{\partial \tilde{c}_m}{\partial z}\bigg|_{z=0} = 0 \tag{2}$$

$$\frac{\partial \tilde{c}_m}{\partial t} - \frac{\tilde{\varepsilon}_t}{\varepsilon}\tilde{D}_p\frac{\partial^2 \tilde{c}_m}{\partial z^2} + \tilde{k}_r\left(\tilde{K}_D \tilde{c}_m - \frac{\rho}{\tilde{\varepsilon}}\tilde{c}_w\right) = 0 \tag{3}$$

$$\frac{\partial \tilde{c}_w}{\partial t} - \tilde{k}_r\left(\frac{\tilde{\varepsilon}}{\rho}\tilde{K}_D\tilde{c}_m - \tilde{c}_w\right) = 0 \tag{4}$$

in which c_m is the dissolved solute mass per unit volume of pore water in the rock matrix [kg/ m^3], c_w is the sorbed solute mass per unit solid mass [kg/kg], D is the molecular (ionic) diffusion coefficient [m^2/s], u is the advection velocity of the solute [m/s], x is a length co-ordinate, h is the fracture aperture [m], E is the hydraulic dispersion coefficient [m^2/s], the pore diffusivity $D_p = D\delta_D/\tau^2$ [m^2/s], ε is the total porosity of rock matrix, ε_t is the porosity of

13

rock matrix available to matrix diffusion, δ_D is the constrictivity, τ is the tortuosity, ρ is the density of the rock [kg/ m^3], the distribution coefficient $K_D = (\rho/\varepsilon) (c_w/c_m)$ and k_r is the sorption rate coefficient [s^{-1}]. Variables marked with a 'tilde' ($\sim$) can be assigned as spatially random in the transport direction (x-direction), if the effects of heterogeneous rock properties are taken into account.

The boundary and initial conditions of a solute pulse traveling in the fracture network are defined as

$$\tilde{c}_m (x = 0, t) = \delta(t) \frac{M_0}{Q} \tag{5}$$

$$\tilde{c}_m (z = 0, t) = \tilde{c}(x, t) \tag{6}$$

$$\left. \frac{\partial \tilde{c}_m}{\partial z} \right|_{z=Z} = 0 \tag{7}$$

$$\tilde{c}(z, t = 0) = \tilde{c}_m (z, t = 0) = 0 \tag{8}$$

in which Q is the water flow [m^3/s], M_0 is the total mass of solute inserted in the fracture [kg], $\delta(t)$ is the Dirac delta function [s^{-1}] and Z is the maximum diffusion depth [m].

If the Laplace transform of a function g is defined as

$$\tilde{g} = L[g] = \int_0^\infty g e^{-pt} dt \tag{9}$$

where L[…] denotes Laplace operator and p is Laplace transform variable, we may readily verify that the temporal moments can be expressed as

$$m_j = (-1)^j \left. \frac{\partial^j \tilde{g}}{\partial p^j} \right|_{p=0} \tag{10}$$

As mentioned in section 2.1, if g(x,t) corresponds to the breakthrough curve, c(x,t), in the fracture, the residence time PDF is defined as $f(x,t) = c(x,t)/m_0$. The central temporal

moments are obtained from the well-known relationships $\mu_t = m_1/m_0$, $\sigma_t^2 = m_2/m_0 - (m_1/m_0)^2$ and $S_t = m_3/m_0 - 3\sigma_t^2\mu_t - \mu_t^3$, in which μ is the expected value [s], σ is the standard deviation (σ^2 is the variance) [s^2] and S is the skewness [s^3].

By using Laplace transforms, e.g. as Maloszewski and Zuber (1990) we can write equations (2) to (4) with corresponding initial and boundary conditions (5) to (8) as

$$\frac{\partial \tilde{\bar{c}}}{\partial x} + \tilde{\beta}(p)\tilde{\bar{c}} = 0 \tag{11}$$

where

$$\tilde{\beta} = \frac{p}{\tilde{u}} - \frac{2\tilde{D}_e}{h\tilde{u}}\tilde{\alpha}\left(1 - \frac{2}{1 + \exp(-2\tilde{\alpha}Z)}\right) \tag{12}$$

$$\tilde{\alpha} = \sqrt{\frac{p\left(1 + \tilde{K}_D\frac{k_r}{p + k_r}\right)}{\tilde{D}_e\tilde{\varepsilon}_t/\tilde{\varepsilon}}} \tag{13}$$

If we neglect the analyses of the effect of uncertainties of rock properties on radionuclide transport at this stage, the solution of (2) to (4) with the boundary and initial conditions (5) to (8) in the Laplace domain is

$$\bar{c} = \frac{M_0}{Q}\exp\left[-\frac{p}{u}x + \frac{2\varepsilon_t D_p}{hu}\tilde{\alpha}\left(1 - \frac{2}{1 + \exp(-2\tilde{\alpha}Z)}\right)x\right] \tag{14}$$

in which p is the Laplace transform variable and

$$\tilde{\alpha} = \sqrt{\frac{p\left(1 + K_D\frac{1}{p + k_r}\right)}{\varepsilon_t/\varepsilon D_p}} \tag{15}$$

Assuming the depth of penetration for matrix diffusion is sufficiently large (Z→∞), standard transforms of (14) yield

$$c(x,t) = \frac{M_0}{Q} \frac{x\varepsilon_t}{uh} \sqrt{\frac{\varepsilon D_p\left(1+\frac{\rho}{\varepsilon}k_d\right)}{\varepsilon_t \pi (t - x/u)^3}} \exp\left(-\frac{x^2 \varepsilon\varepsilon_t D_p\left(1+\frac{\rho}{\varepsilon}k_d\right)}{u^2 h^2 (t - x/u)}\right)\theta(t - x/u) \tag{16}$$

2.3 Deterministic analysis of solute transport with spatially variable rock properties

A purpose of this section is to analyse the effect of a deterministic (known) variability of rock properties on the solute transport in a single fracture. Such a solution is important in order to understand the different effects of parameter heterogeneity related to the spatial variability of parameters along a specific transport path.

For simplicity we start by considering a fracture that is divided in two parts of equal size. We can obtain the solution S at the distance x=X by using the solution from the first half (x=X/2) as a boundary condition for solving the transport in the second half. Formally, the solution can be expressed as a convolution $S = S_1*S_2$, where the subscripts 1 and 2 denote the first and second halves of the fracture and * is the convolution operator. Since $L[S_1*S_2]=L[S_1]L[S_2]$, (14) implies that

$$\bar{c} = \frac{M_0}{Q} \exp\left[-\frac{p}{u_1}\frac{X}{2} + \frac{2\varepsilon_{t,1}D_{p,1}}{h_1 u_1}\alpha_1\left(1 - \frac{2}{1+\exp(-2\alpha_1 Z_1)}\right)\frac{X}{2}\right]$$

$$\exp\left[-\frac{p}{u_2}\frac{X}{2} + \frac{2\varepsilon_{t,2}D_{p,2}}{h_2 u_2}\alpha_2\left(1 - \frac{2}{1+\exp(-2\alpha_2 Z_2)}\right)\frac{X}{2}\right] \tag{17}$$

where L[…] is the Laplace transform. If we assume an infinite rock matrix (Z→∞) the inverse transform of (17) is

$$c(x,t) = \frac{M}{Q}\int_0^\infty \frac{X/2\, \varepsilon_{t2}}{u_2\, h_2} \sqrt{\frac{\varepsilon_2\, D_{p2}\,(1+K_{D2})}{\pi\,(t-\tau-(X/2)/u_2)^3 \varepsilon_{t2}}} \exp\left[-\frac{\varepsilon_{t2}\,\varepsilon_2\, D_{p2}\,(1+K_{D2})\,(X/2)^2}{h_2^2\, u_2^2\,(t-\tau-(X/2)/u_2)}\right]\theta(t-\tau-(X/2)/u_2)$$

$$\frac{X/2\,\varepsilon_{t1}}{u_1\,h_1}\sqrt{\frac{\varepsilon_1\,D_{p1}\,(1+K_{D1})}{\pi\,(t-(X/2)/u_1)^3\varepsilon_{t1}}} \exp\left[-\frac{\varepsilon_{t1}\,\varepsilon_1\,D_{p1}\,(1+K_{D1})\,(X/2)^2}{h_1^2\,u_1^2\,(t-(X/2)/u_1)}\right]\theta(t-(X/2)/u_1)\,d\tau$$

$$\tag{18}$$

We can see directly from convolution principles that the convolution (18) is identical to the convolution in which the solutions S_1 and S_2 are interchanged with each other; i.e. $S_1 * S_2 = S_2 * S_1$. The implication is that the spatial order of the two halves does not affect the convoluted solution. However, the variance of the properties affects the solution. Since the different properties form a lumped parameter F that is a function of the different variables $F(K_D; \varepsilon; \varepsilon_t; u; h)$, we cannot unconditionally use the expected values of the individual parameters, i.e. $E[F] \neq F(E[K_D]; E[\varepsilon]; E[\varepsilon_t]; E[u]; E[h])$. This is because of both possible cross-covariance between parameters and the fact that the expected value of a function of a single stochastic variable is not generally the function of the expected value of the stochastic variable.

The convolution can be performed for any arbitrary number of parts of any arbitrary lengths, which means that the above conclusions can even be generalised to a network scale. Consequently, if we were able to take samples from the bedrock to the extent that we are sure what properties migrating radionuclides will encounter, the auto-correlation of a rock property would not be important for the solution. However, the variance of the properties is important for the solution. Fig. 1 shows how the solution varies between a case in which when we consider the variance in the properties (solution is obtained as $E[S]$) and when the properties are represented using expected values (solution is obtained as $S(E[K_D]; E[\varepsilon]; E[\varepsilon_t]; E[u]; E[h])$). The difference is generally not so great even if all properties vary and, for moderate variances, we can use the expected values of the properties as approximations.
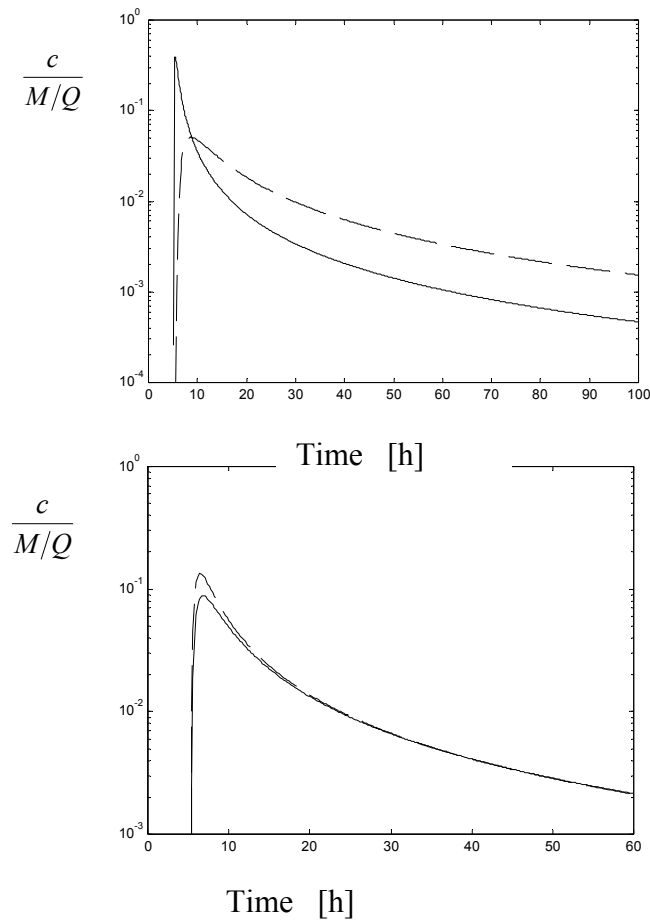
Fig. 1 *Solution according to (18) to transport in a fracture in which the properties are different in two half-parts (solid curves) and the solution according to (16) with expected value of the individual parameters (dashed curve). In the left-hand diagram the effective diffusivity D_p varies a factor 10 between the two half-parts. In the right-hand diagram the fracture aperture h varies a factor 10 between the two half-parts. The largest values of D_p and h were $1x10^{-9}$ m^2/s and $2x10^{-3}$ m. Further, u = 0.198 m/h, K_D = 540, ε_t = 0.004 and ε = 0.006.*

2.4 Evaluation of Covariance Structures of Transport Properties of Crystalline Rock and Implications to Solution Procedure

An important problem for interpretation of modelling results is due to the fact that measuring programmes generally provide discrete information on a large set of physical and geochemical parameters. The discrete data sampling leads to a need to "interpolate" between known data and this introduces significant uncertainties in a transport analysis

similarly as there is an uncertainty in the water flow analysis. The uncertainty analysis is based on theory for stochastic processes and further discussed in section 2.5. One of the key statistical measures that appear in the stochastic analysis is the auto-covariance function of the different rock properties. This section focuses on how auto-covariance of the different properties can be expressed in terms of the auto-covariance of the auxiliary variable β and how this can be related to data.

Since the matrix properties are nested with each other and with the Laplace variable p in (13), the auto-covariance of the β can be rather complicated when equated in terms of the auto-covariances of the individual rock properties. Here we will explore the approximation using a "Simple Approach" (Wörman et. al., 2003), which is to assume that the *stochastic components* of the β are represented as if the sorption kinetics is rapid ($k_r \rightarrow \infty$) and the permissible depth of matrix diffusion is infinite ($Z \rightarrow \infty$). The approximation is reasonable for short transport distances, because then perturbations introduced inside the exponential function of (12) contributes only insignificantly to the perturbations in the β. Hence, the stochastic components of the β can be isolated in three factors $\eta_u(x)$, $\eta_h(x)$ and $\eta_M(x)$ containing $\tilde{\varepsilon}, \tilde{\varepsilon}_t, \tilde{D}_p, \tilde{h}, \tilde{u}$ and $\tilde{K}_D$, where $\eta_u \equiv u/\tilde{u}$, $\eta_h \equiv h/\tilde{h}$, $\eta_M \equiv \tilde{M}/M$, $M = (D_p \varepsilon_t \varepsilon (1+K_D))^{0.5}$ [m s$^{-0.5}$] and variables without 'tilde' are expected values (e.g. u = E[$\tilde{u}$]). We may rewrite (12) as

$$\tilde{\beta} = c_1 \eta_u + c_2 \eta_u \eta_h \eta_M \tag{19}$$

in which c_1 and c_2 are defined in Table 1.

According to the derivation in Appendix 2, the auto-covariance of β defined according to (19) will contain seven auto-covariance terms (A2-4). The auto-covariance of β also includes a large number of cross-covariances that could readily (from an analytical point of view) be included in the analysis, especially, if they are written in a form appropriate for the convolution integral (27). How many terms should be included in the series is a matter of judging the importance of the terms and practical possibilities of measuring the individual factors. The solution of the convolution integral (27) is not obstructed significantly, however, by the number of terms considered. Nor is the moment

19

calculation or the Laplace inversion, since the Laplace variable 'p' has been separated from the η´s in (19).

In this study, we neglect the cross-covariances due to the lack of relevant data and the extensive administrative task of accounting for the cross-covariances described in Appendix 2 and especially their contributions to the a_i-factors in Table 1. Further, the cross-covariances are always smaller than the auto-covariance of an individual factor and, therefore, of lesser importance.

Geostatistics of fracture apertures and rock properties such as porosity, effective diffusivity and sorption capacity were investigated by Hakami and Barton (1990) and Xu & Wörman (1998) on rock samples taken from Äspö Hard Rock Laboratory in Sweden. Both investigations show that the auto-covariance functions of aperture and effective matrix parameter can be described by an exponential function. Thus, the covariance function β can be expressed as a series of exponential functions with different a_i and correlation length ℓ_i corresponding to the different rock properties:

$$\mathrm{Cov}\big[\tilde{\beta}(s)\big] = \sum_{i=1}^{7} a_i e^{-s/\ell_i} \tag{20}$$

where a_i and ℓ_i are defined in Table 1.

Table 1 *Definition of typical coefficients in Eqs. (19) and (20). The α is defined based on expected values of the included parameters.*

$c_1 = \dfrac{p}{u}$		$c_2 = -\dfrac{2\varepsilon_t D_p}{hu}\alpha\left[1 - \dfrac{2}{1+\exp(-2Z\alpha)}\right]$	
i	a_i	b_i	ℓ_i
1	$(c_1 + E[\eta_h]E[\eta_M]c_2)^2 b_1$	$\mathrm{Var}[\eta_u]$	ℓ_u
2	$(c_2)^2 b_2$	$E^2[\eta_u]E^2[\eta_M]\mathrm{Var}[\eta_h]$	ℓ_h
3	$(c_2)^2 b_3$	$E^2[\eta_u]E^2[\eta_h]\mathrm{Var}[\eta_M]$	ℓ_M
4	$(c_2)^2 b_4$	$E^2[\eta_u]\mathrm{Var}[\eta_h]\mathrm{Var}[\eta_M]$	$\dfrac{1}{1/\ell_h + 1/\ell_M}$
5	$(c_2)^2 b_5$	$E^2[\eta_h]\mathrm{Var}[\eta_u]\mathrm{Var}[\eta_M]$	$\dfrac{1}{1/\ell_u + 1/\ell_M}$
6	$(c_2)^2 b_6$	$E^2[\eta_M]\mathrm{Var}[\eta_u]\mathrm{Var}[\eta_h]$	$\dfrac{1}{1/\ell_u + 1/\ell_h}$
7	$(c_2)^2 b_7$	$\mathrm{Var}[\eta_u]\mathrm{Var}[\eta_h]\mathrm{Var}[\eta_M]$	$\dfrac{1}{1/\ell_u + 1/\ell_h + 1/\ell_M}$

2.5 Methodology of solving one-dimensional stochastic solute transport problem

This section focuses on using the spectral method to obtain solutions of the stochastic transport problem both in terms of a closed-form solution in Laplace domain (following the method outlined in section 2.2) and temporal moments of the travel time PDF. The temporal moments of the travel time PDF are generally considered to be typical quantities of solute transport and are often obtained by the way of Laplace transforms (e.g. Espinoza and Valocchi, 1997). The temporal moments can be interpreted as "effective" transport properties such as mean residence time and variance of the residence times and are suitable for incorporation in large-scale transport models or directly in the safety assessments of the nuclear waste repository (Cvetkovic and Selroos, 1999).

By defining $\tilde{\beta}(p)$ as a stochastic variable we define the stochastic properties of (11) as the sum of their expected value (or ensemble average), denoted by E[...], and random perturbations deviating around the mean, denoted by a prime;

$$\tilde{\beta}(p,x) \equiv E\left[\tilde{\beta}(p,x)\right] + \beta'(p,x) \tag{21}$$

$$\bar{c}(p,x) \equiv E\left[\bar{c}(p,x)\right] + \bar{c}'(p,x) \tag{22}$$

The definition (21) implies that

$$E\left[\beta'\right] = 0 \tag{23}$$

Similarly, we have E[$\bar{c}'$] = 0. In terms of perturbations the governing equation (11) can thus be written as

$$\frac{\partial E[\bar{c}]}{\partial x} + \frac{\partial \bar{c}'}{\partial x} + E\left[\tilde{\beta}\right]E[\bar{c}] + E\left[\tilde{\beta}\right]\bar{c}' + \beta'E[\bar{c}] + \beta'\bar{c}' = 0 \tag{24}$$

The expected value of (24) under consideration of (23) yields

$$\frac{\partial E[\bar{c}]}{\partial x} + E[\tilde{\beta}]E[\bar{c}] + E[\beta'\bar{c}']_{s=0} = 0 \tag{25}$$

in which s is the separation distance between the locations along the x-direction of β' and $\bar{c}'$. Expression of the cross-covariance between β' and $\bar{c}'$ (for s=0) is known as the "closure problem".

A perturbation equation is obtained by subtracting (25) from (24);

$$\frac{\partial \bar{c}'}{\partial x} + E[\tilde{\beta}]\bar{c}' + \beta'E[\bar{c}] + \beta'\bar{c}' - E[\beta'\bar{c}']_{s=0} = 0 \tag{26}$$

The last two terms of (26) representing perturbations of second order can be omitted if their sum is small in comparison to other terms of the equation (e. g. Espinoza and Valocchi, 1997). Therefore, the last two terms of (26) are neglected in the subsequent analysis.

By using a spectral representation (Fouries-Stiltjes integrals) of the stochastic variable of (26) we can derive the expression of the cross-spectral density function of β' and $\bar{c}'$ in Fourier-space (Appendix 1). Transformation to the real domain yields:

$$Cov[\beta'(x+s),\bar{c}'(x)] = -E[\bar{c}] \int_{-\infty}^{\infty} \beta'(s-\zeta)e^{-E[\tilde{\beta}](s-\zeta)}Cov[\beta'(s=\zeta)]d\zeta \tag{27}$$

in which $\theta(s)$ is the Heaviside unit function, ζ is the convolution integrand and $cov[\beta'(s)]$ is a short form of $cov[\beta'(x),\beta'(x+s)]$ that is used under the assumption of stationarity of the covariance function. As before, s is the separation distance along the x-direction.

If (20) is inserted in (27), we obtain

$$Cov[\beta'(x),\bar{c}'(x)]_{s=0} = E[\beta',\bar{c}']_{s=0} = -E[\bar{c}]\sum_{i=1}^{7} a_i \frac{\ell_i}{E[\tilde{\beta}]\ell_i + 1} \tag{28}$$

22

in which the amplitudes a_i and the correlation lengths ℓ_i are defined in Table 1. The solution of (25) and (28) using the boundary condition (7) becomes

$$E[\overline{c}] = \frac{M_0}{Q} \exp\left[\left(-E[\tilde{\beta}] + \sum_{i=1}^{N} a_i \frac{\ell_i}{E[\tilde{\beta}]\ell_i + 1}\right)x\right] \tag{29}$$

in which N=7 for the solution in a single fracture and N=26 for the solution in a network scale.

The uncertainty of the mean value solution can be expressed from the solution of the perturbation equation (26). By substituting (29) in (26) and using the boundary conditions $\overline{c}'(x = 0) = 0$, we may derive

$$\overline{c}' = \frac{M_0\beta'}{Q\sum_{i=1}^{N} a_i \frac{\ell_i}{E[\beta']\ell_i + 1}} \exp\left(-E[\tilde{\beta}]x\right)\left(1 - \exp\left(\sum_{i=1}^{N} a_i \frac{\ell_i}{E[\tilde{\beta}]\ell_i + 1}\right)\right) \tag{30}$$

in which β' is defined in Appendix 2.

Unfortunately, this solution in the Laplace domain cannot be inverted in closed form according to the best of the authors' knowledge. Therefore, the series expansion method of De Hoog et al. (1982) was applied in a numerical inversion algorithm using the MATLAB® code written by Hollenbeck (1998). The accuracy of the numerical inversion was tested by means of comparisons with a closed-form solution (Neretnieks 1980) for the case with homogeneous parameters and equilibrium sorption.

The application of (10) to (29) involves a series of tedious but also relatively simple operations, which lead to the following expressions for the central temporal moments:

$$\mu_t = \frac{x}{u} E[\eta_u]\left(1 + E[\eta_h]E[\eta_M]R\right) \tag{31}$$

$$\sigma_t^2 = \frac{2}{3}\frac{x}{u}RTE[\eta_u]E[\eta_h]E[\eta_M]\left[1 + \Psi_1 + 3R\left(\frac{(1+E[\eta_h]E[\eta_M]R)^2}{R^2}\sum_{i=1}^{N_1}H_i + \sum_{i=N_2}^{N_3}H_i\right)\right] \quad (32)$$

$$S_t = \frac{4}{5}\frac{x}{u}RT^2E[\eta_u]E[\eta_h]E[\eta_M]\left[1 + 5\Psi_1\Psi_2 + \frac{5}{2}\frac{(1+E[\eta_h]E[\eta_M]R)}{R}\sum_{i=1}^{N_1}H_i\right.$$
$$\left(3E^2[\eta_u]E[\eta_h]E[\eta_M]\sum_{i=1}^{N_1}\frac{H_i}{b_i}(1+E[\eta_h]E[\eta_M]R)^2 + 2E[\eta_h]E[\eta_M]R(1+\Psi_1)\right) +$$
$$\left. +\frac{5}{2}\sum_{i=N_2}^{N_3}\left(H_i\left(3\frac{H_i}{b_i}E^2[\eta_u]E[\eta_h]E[\eta_M](1+E[\eta_h]E[\eta_M]R)R + 2R + 2R\Psi_1\right)\right)\right] \quad (33)$$

in which $N_1=1$, $N_2=2$ and $N_3=7$ for the solution in a single fracture and $N_1=2$, $N_2=3$ and $N_3=26$ for the solution in a network scale, the typical parameters R, T, Ψ_1, Ψ_2 and H_i are defined in Table 2, all of which are expected values. The effect of the uncertainty of the parameters in a heterogeneous bedrock is reflected in the H-parameters. The $E[\eta_i]$ coefficients represent the effect of the actual (known) variability in parameters that exists even if there is no uncertainty about the distribution of properties along a specific transport path. The homogeneous case is obtained for $H_i = 0$; $i = 1,2\ldots7$. The ψ–parameters reflect the kinetics of the sorption process and can be disregarded in the case of equilibrium sorption ($\psi_1 \ll 1$).

From (31), the travel velocity is linearly proportional to the advection velocity according to $dx/d\mu_t = u/(1 + R)$, in which R can be interpreted as a retardation factor. The retardation coefficient reflects the mass ratio of the solute that on the average is resident in the rock matrix and the main fracture, respectively. The variance of the travel time PDF increases linearly with the retardation coefficient and the typical residence time, T, for the solute in the rock matrix. From (31) we may also conclude that the heterogeneity of the problem parameters (fracture aperture, fracture velocity, matrix diffusivity, bedrock porosity and sorption partition coefficient) does not affect the mean residence time. However, there is a corresponding positive contribution to both the variance and the skewness of the residence time.

Table 2 *Definition of typical parameters governing the propagation of a solute pulse in a fracture.*

$$R = \frac{2Z\varepsilon}{h}(1 + K_D) \qquad\qquad T = \frac{\varepsilon}{\varepsilon_t}\frac{Z^2}{D_p}(1 + K_D)$$

$$\Psi_1 = \frac{3K_D}{Tk_r(1 + K_D)} \qquad\qquad \Psi_2 = \frac{K_D}{3(1 + K_D)} + \frac{1}{2Tk_r} + \frac{1}{3(1 + K_D)}$$

$$H_i = \frac{\ell_i\, b_i}{E[\eta_u]E[\eta_h]E[\eta_M]\,u\,T} \quad \text{where } \ell_i \text{ and } b_i \text{ are defined in Table 1 and Table}$$

A3-1 depending on the solution if it is for single fracture or network scale.

2.6 Extending the solutions to a network scale

The convolution integral (1) can be applied to a distribution of pathways both in a two dimensional fracture and in a network or a two-dimensional fracture network. The latter problem is more general and, therefore, focused on in this section.

Fig. 2 presents a schematic of the variation of β along the network of fractures and illustrates the shift of the local mean values of β between fractures around the mean value of β for the whole network. In addition, within each fracture the β varies around its mean value. Hence, the perturbation of β in (21) includes two parts:

$$E\left[\tilde{\beta}(p,x)\right] + \beta' \equiv E\left[\tilde{\beta}(p,x)\right] + \beta'_n(p,x) + \beta'_s(p,x) \qquad\qquad (34)$$

in which β'_n denotes a random perturbation of the mean value of individual fractures around the mean aperture of the ensemble of fractures and β'_s denotes the random perturbation around the mean value of the individual fracture (Fig. 2).

To solve (11) with β expressed according to (34) we can follow exactly the same procedures as described before. However, the expression of covariance of $\beta'(s)$ will be 26 terms instead of 7 terms according to the derivation of Appendix 3. The solutions are given on the same form as (31), (32) and (33), but the expected values of various parameters are defined as mean values of the network and the H-parameters are defined in Table 2 and Table A3-1 in Appendix 3.
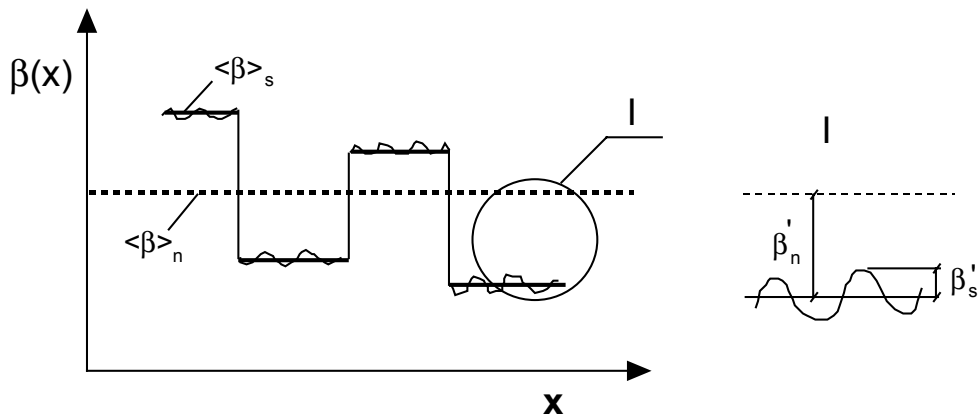
Fig. 2 *Definition sketch of perturbation of β along the pathway in a fracture network, in which, $<\beta>_s$ denotes the mean value of the single fracture, $<\beta>_n$ denotes the mean value of the ensemble of fractures in the network, β'_n and β'_s denote the perturbation around $<\beta>_n$ and $<\beta>_s$ respectively.*

2.7 One-Dimensional Continuum Model

Section 3.4 contains a comparison in result between the multi-dimensional description of the water flow and solute transport, explored in this study, and the classical one-dimensional continuum description of solute transport by groundwater as given by the Advection-Dispersion equation. This comparison is introduced to demonstrate the importance of the multi-dimensional approach for certain field conditions. For a continuous Darcy velocity field, the one-dimensional solute transport mechanism can be described by [*SKI*, 1996],

Mobile phase in pore water

$$\frac{\partial c}{\partial t}(\theta R c) + q\frac{\partial c}{\partial x} - \frac{\partial}{\partial x}\left(\theta D \frac{\partial c}{\partial x}\right) = a\theta_m D_m \frac{\partial}{\partial z}c_m\big|_{z=0} - \lambda\theta R c \qquad (35)$$

Immobile phase in the rock matrix

$$\frac{\partial}{\partial t}(R_m c_m) = D_m \frac{\partial^2 c_m}{\partial z^2} - \lambda R_m c_m \qquad (36)$$

were the retardation factors due to surface sorption and sorption into the rock matrix is defined

$$R = 1 + \frac{k_{d,f}\rho(1-\theta_m)a\delta}{\theta} \qquad (37)$$

$$R_m = 1 + \frac{k_d\rho(1-\theta_m)}{\theta_m} \qquad (38)$$

and

c = concentration of radionuclide i in the pore water [kg/m^3]
c_m = concentration of radionuclide i in the matrix water [kg/m^3]
q = groundwater flow (Darcy velocity) [m^3/ m^2/s]
D = dispersion coefficient for porous media [m^2/s]
a = specific flow wetted area of fractures (per volume rock mass) [m^{-1}]
w = distance into matrix orthogonal to fracture surface [m]
D_m = matrix diffusivity [m^2/s]
$k_{d,f}$ = sorption coefficient for radionuclide i for the fracture surfaces [m^3/kg]
k_d = sorption coefficient for radionuclide i inside rock matrix [m^3/kg]
δ = 'depth' of surface sorption [m]
θ = rock mass ('flowing') porosity [-]
θ_m = matrix porosity [-]

λ_i = decay constant for radionuclide i [s^{-1}]
ρ_m = bulk density of rock matrix [kg/ m^3]

      With the same initial and boundary conditions as (5) to (8) a solution to equations (35) and (37) can easily be found in the Laplace domain following a series of simple steps:

$$\overline{c} = \frac{M}{Q} \exp\left(\frac{qx}{2\theta D}\left(1 - \sqrt{1 + \frac{4D\theta^2}{q^2}\left[R(p+\lambda) - \frac{a\theta_m D_m}{\theta}\alpha\left(1 - \frac{2}{1+\exp(-2\alpha z)}\right)\right]}\right)\right) \quad (39)$$

where the auxiliary variable is defined as

$$\alpha = \sqrt{\frac{R_m(p+\lambda)}{D_m}}$$

The inversion of equation (39) to the real time domain cannot be obtained analytically to the best of the author's knowledge. Instead, a solution is obtained with a numerical inversion algorithm based on the series expansion method of De Hoog et al., (1982).

3. Illustrative application based on a discrete-feature model

For the purpose of illustrating the travel-time approach and comparing with the 1-D continuum model for transport, in this chapter illustrative cases are developed based on a 3-D discrete-feature model that was developed and tested in SKI's SITE-94 performance-assessment study (SKI, 1996).

Monte Carlo simulations of the flow field and particle tracking is used to obtain the expected value of the residence time PDF, $g(\tau)$, of inert water parcels travelling through fracture networks from damaged canisters and to discharge locations. The transport paths for a non-sorbing, conservative tracer, not affected by matrix diffusion, are calculated by the discrete-parcel random-walk method. Based on the residence time PDF obtained from the particle tracking procedure, the water flow is coupled with the solute transport analyses of section 2.5 using the method of section 2.1. The information obtained by this approach is also translated to hydrological parameters used in the one-dimensional continuum modelling (i.e. Darcy velocity, effective longitudinal dispersion coefficient, flow porosity and flow wetted surface).

Examples of hydrological properties derived from the simulations of transport in the fracture network are illustrated in section 3.2. A comparison of the two approaches is performed in section 3.3. This section also focuses on effect of uncertainty in heterogeneous rock properties on radionuclide transport. A combination of effect of flow and uncertainty due to heterogeneous rock properties is discussed in section 3.4.

3.1 Discrete-feature model for water flow analysis

The 3-D discrete-feature (DF) model used in this application consists of three major types of components [Geier, 1996]: 1) large-scale transmissive structures, including fracture zones and single fractures more than 50 m in extent, 2) smaller-scale fractures in the vicinity of the repository, and 3) man-made hydrologic features in the repository, including the disturbed-rock zone (DRZ) around the repository tunnels and shafts (see Fig. 3).

The large-scale structures along with the man-made features are treated as deterministic with respect to geometry (i.e. the coordinates of these features are fixed in all

realisations of the model), and with hydraulic properties that may be treated as either deterministic or stochastic depending on the calculation case.

The small-scale fractures are treated as a stochastic population of disc-shaped fractures (approximated by polygons in the model), defined in terms of a stochastic process for the location of fracture centers, and statistical distributions for other fracture properties (e.g. radius, orientation, and transmissivity). Realizations of the small-scale fracture population are generated by unconditional Monte Carlo simulation.

For each calculation case, multiple realizations of the integrated model are formed by combining realizations of the smaller-scale fracture population with the large-scale features. For each realization, the DF model is assembled and discretized to produce a finite-element mesh, composed of triangular elements, which represents all connections among the discrete features. Boundary conditions (fixed-head, fixed flux, or fixed net flow) are imposed at the intersections between the discrete features and the model boundaries.

The steady-state hydraulic head field resulting from the prescribed boundary conditions is calculated for each realization by the Galerkin finite-element method. The velocity $\boldsymbol{u}$ within each element is calculated from the hydraulic head distribution as:

$$\mathbf{u} = \frac{-T\nabla H}{h_T} \tag{40}$$

where H is the hydraulic head, T is the transmissivity of the element, and h_T is an effective aperture which is assumed to be related to the element transmissivity.
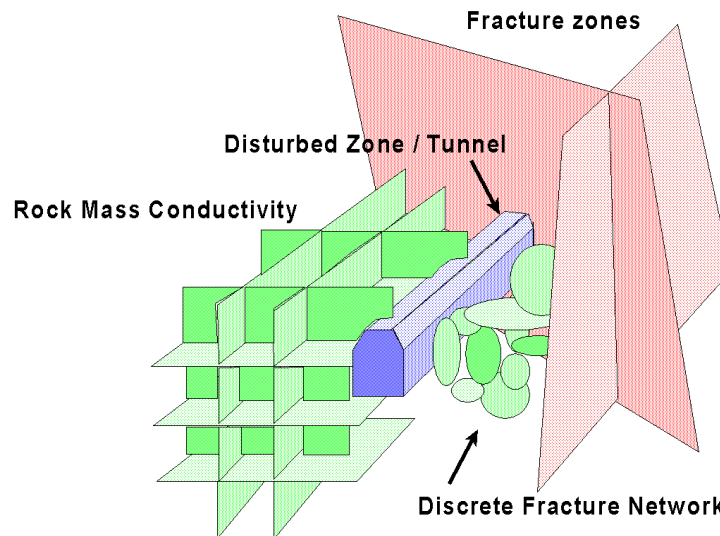
Fig. 3 *Components of the SITE-94 discrete-fracture model (Geier, 1996).*

3.2 Simulations of hydrological properties of a discrete-fracture network

The demonstration case presented in this section is based on a 3-D discrete-feature model of a 5 km by 5 km area, 1 km deep and geological information obtained from the Äspö Hard Rock Laboratory site in south-eastern Sweden (Geier, 1996). Large-scale, deterministic features in the model represent regional and local-scale fracture zones that were identified by interpretation of topographical and aerial geophysical data, combined with ground-based geophysics and borehole data. A few of these features which are intersected by boreholes have been characterized by hydrologic tests, including one suite of radially convergent tracer tests, which help to constrain the flow and transport properties of these features.

The smaller-scale fracture population in the detailed portion of the model is described based on statistical interpretation of fracture geometry data from outcrops and boreholes, and detailed hydrologic testing in boreholes. Statistical summaries of the fracture populations in the two main lithologic types in this location are given in Table 3. In both cases, analysis of fracture data indicated that nonuniform clustering of fractures cannot be described as a uniformly random Poisson process for fracture center location, but is more closely

Table 3. *Statistical summary of models for fracturing in the repository block. Orientation distributions are defined by bootstrap resampling of Terzaghi-corrected datasets, for all fracture sets.*

Rock Type	Fracture Set	Fracture location		Fracture transmissivity Lognormal		Fracture radius Power-law
		D_{LL} (-)	P_{32c} (m^2/m^3)	$\lambda_{\log T}$ (log$_{10}$ m^2/s)	$\rho_{\log T}$ (log$_{10}$ m^2/s)	b_r (m)
Äspö granodiorite	All	2.23	0.799	-8.5	1.0	-
	1		0.314			3.00
	2		0.163			3.01
	3		0.138			2.74
	4		0.184			2.55
Småland granite	All	2.14	0.427	-8.0	1.25	-
	1		0.159			3.00
	2		0.086			3.01
	3		0.082			2.74
	4		0.100			2.55

approximated by a fractal (3-D Levy flight) process, which is characterized in terms of a fractal dimension D_{LL} for the point field of fracture centers. The intensity of fracturing in the models is described in terms of the total interfacial area of conductive fractures per unit volume of rock, P_{32c} [m^2/m^3].

Four fracture sets were identified based on orientation: (1) NW to NNW strike, steeply dipping, (2) NE strike, steeply dipping, (3) subhorizontal, and (4) N-S strike, steeply dipping. The orientations of the simulated population of fractures were generated by bootstrap resampling of fracture pole data from outcrop mapping, after a correction for directional sampling bias.

Fracture transmissivity for all sets was modeled by a lognormal distribution, estimated by forward modeling of the observed distribution of 3 m section transmissivities based on the inferred model for fracture clustering. Thus transmissivity was assumed to be independent of orientation and fracture size.

Fracture size (i.e. the radius of the discs) for all four fracture sets, for both rock types, was found to follow a power-law distribution. Thus both the fracture size distribution and fracture location process were inferred to have self-similar (fractal) properties, although it was not positively demonstrated that the fracture population as a whole was a fractal.

This statistical model was partly verified by simulation of transient hydraulic tests on 3 m sections, which showed that the model reproduced the observed distributions of both section transmissivity and flow dimension. However, it seems likely that other combinations of statistical parameters could also reproduce these attributes ofthe fracture network. Thus this model should be regarded as one in a locus of possible models that have the capacity reproduce, in a statistical sense, the transient behavior of the fracture network over the scale affected by these hydraulic tests (likely a few meters).

For particle-tracking runs, the effective transport aperture b_T in the stochastic fracture population was also required. A correlation to hydraulic aperture b_h was assumed, based on a regression analysis of single-fracture flow and transport experiments in the literature:

$$b_T \ = \ 10^{-1.35} \, b_h^{0.44}$$

where both apertures are in units of meters, and where b_h is by definition calculated from the fracture transmissivity T according to the cubic law:

$$b_h = (12 \lambda T / \theta g)^{1/3}$$

where λ and θ are the viscosity and density of water, respectively.

The model also includes conductive features associated with the backfilled shafts and tunnels of a hypothetical repository located under the island of Äspö (Figure 4). The entire repository layout was included in the model for the purpose of modelling fluid flow within and around the repository, but only 40 of the spent-fuel canister locations in this repository were modeled as potential sources of radionuclides for transport modelling as described below.
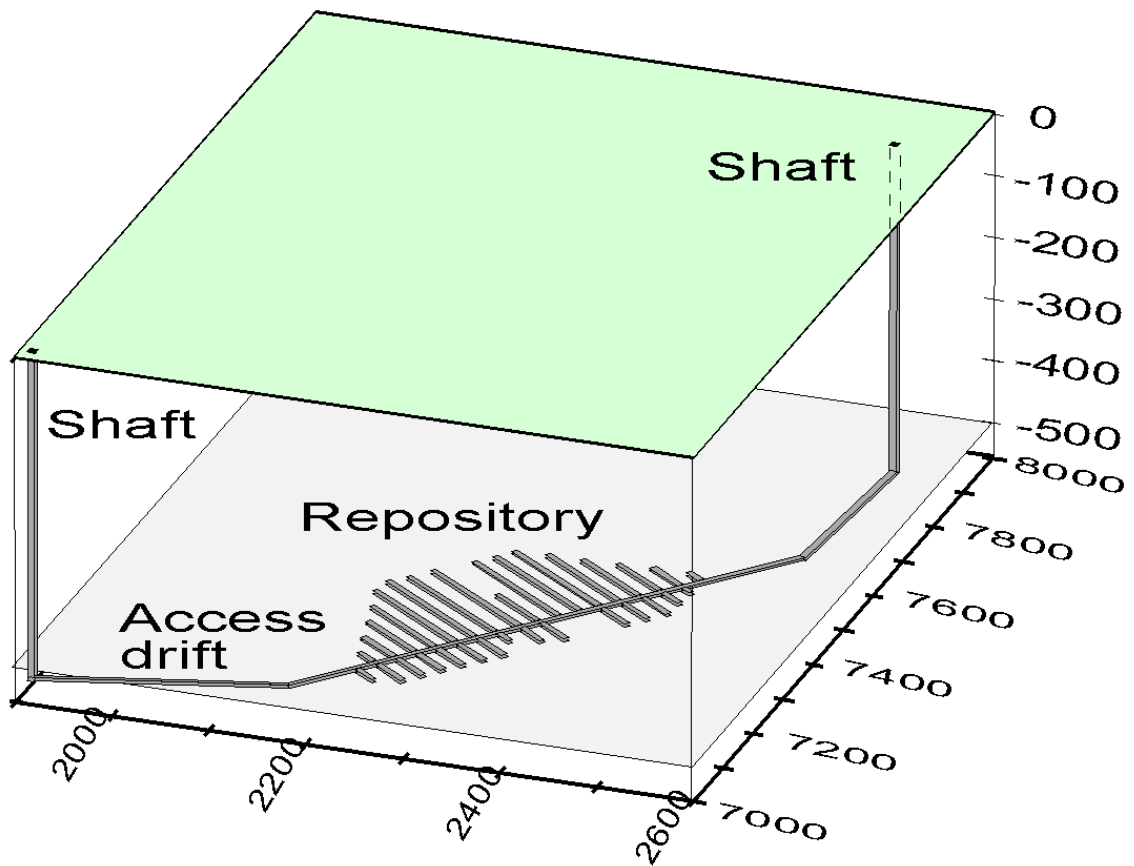
Fig. 4 *Layout of shafts, access tunnels, and deposition tunnels for spent-fuel canisters, in the hypothetical repository considered in the discrete-feature modelling example.*
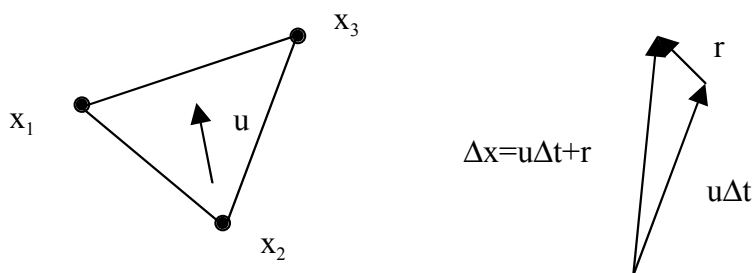
Fig. 5 *Representation of the advective-dispersive motion in a single step of the DPRW algorithm, within a single, linear finite element.*

For each realization of the flow field and for each of forty spent-fuel canister locations (deposition holes), the discrete-parcel random-walk (DPRW) method was used to model advective-dispersive transport through water-conducting features in the discrete-feature model. Particles were tracked from the deposition hole boundary until they crossed a monitoring horizon 50 meters below the ground surface, at which point the radionuclide particles were considered to have reached the biosphere for the purposes of the SITE-94 safety-assessment exercise.

Forty canister locations act as potential sources in a hypothetical repository. Particles representing arbitrary masses of solute are released along the edges of fractures that intersect the deposition holes. The initial positions of the particles are chosen randomly and in proportion to the flow-rate exiting in the deposition hole through each fracture, relative to the total flow through the deposition hole.

The motion of a particle within an element is modeled as a 2-D random walk (Fig. 5). Since in the discrete-feature model the aperture is modelled as a having a constant value within a given element (assumed to represent an effective average over that scale), the random walk is used to account for local hydrodynamic dispersion resulting from the combined effects of molecular diffusion, shear dispersion, and heterogeneity of physical aperture on smaller scales.

In the random walk, the displacement of the particle Δx for a given time step Δt is the vector sum of a deterministic, advective component $u\Delta t$ and a random, dispersive component r. Here u is the local fluid velocity (assumed to be an average over the scale of the element). The time step Δt for each increment of particle motion in the random walk is chosen based on the ratio of fluid velocity to element size.

The dispersive component r is a random vector sampled from a bivariate normal distribution of displacements from the origin, with principal components aligned with the longitudinal (parallel to flow) and transverse directions, and component variances equal to $2D_L\Delta t$ and $2D_T\Delta t$, respectively. The dispersion coefficients D_L and D_T are assumed to be functions of the magnitude of the local velocity (de Marsily, 1986):

$$D_L = \max(\alpha_L |u|, D_m) \tag{41}$$

$$D_T = \max(\alpha_T |u|, D_m) \tag{42}$$

where α_L and α_T [m] are the longitudinal and transverse dispersivities, respectively, within a given fracture, and D_m is the coefficient of molecular diffusion (0.02×10^{-9} m^2/s for common ions in water).

The ratio α_T/α_L is assumed to be constant through out the network. For the transport simulations described below, α_T/α_L is set equal to 0.1. This value is within the typical range of 0.01 to 0.2 in porous media (Marsily, 1986). If α_L is known D_L and D_T can be calculated according to (41) and (42). Determination of α_L will be discussed in Chapter 4.

3.3 Extraction of parameters for one-dimensional solute transport

Parameters for one-dimensional solute transport models can be extracted straightforwardly from a hydrologic model, by recording the particle position x and the local parameter values of interest (T, h, u) as functions of x for discrete time intervals and then using the statistics of these along with the inert-particle travel time distributions as input to the one-dimensional model.

As a simplest case, parameters can be deduced from hydrologic scoping calculations based on simplifying assumptions. Fig. 6 shows the result of g(τ) taken from SITE-94 far field scoping calculation case 1a3 (SKI, 1996, p497). This scoping calculation is based on a highly simplified model of hydrology, which considers just the possible range of head differences at the site, and effectively 1-D flow and transport paths with homogeneous properties.

More complex travel-time distributions can result from 3-D flow systems in a fracture network. Branching and multiply-connected pathways within a network (which might possibly be coupled by lateral diffusion within fractures and mixing at fracture intersections, even though the paths represent different streamlines) can give rise to more complicated travel-time distributions. Figure 7 shows a case with multi-peak behaviour giving distinctly different travel times for different fractions of the particles released from a single source canister.

g(τ)

Time   [years]
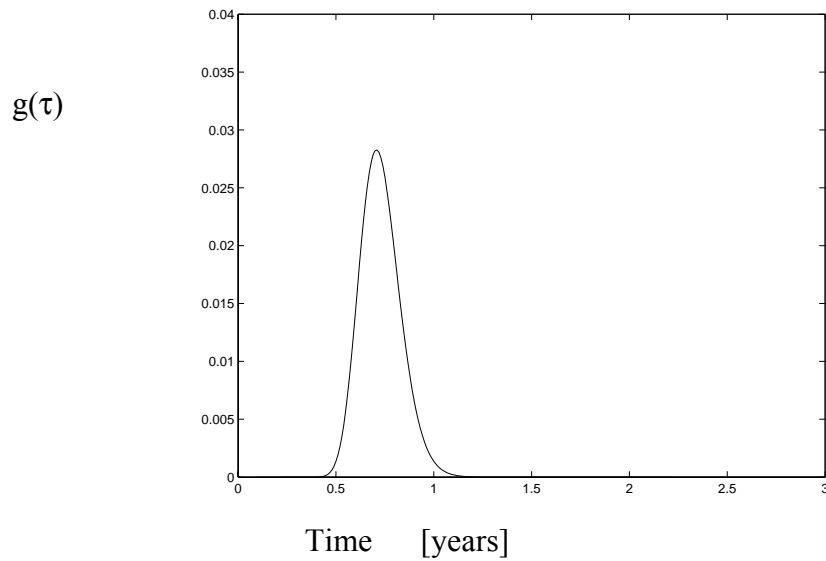
Fig. 6 *Residence time PDF of inert water parcels from a single canister through the fracture network to the biosphere, in which x=100 m, u=140 m/y and E=140 m²/y. The curve is fitted to results obtained in SITE-94 far field scoping calculation cases 1a3 (SKI, 1996, p. 497)*

Cumulative probability density

Time   [years]
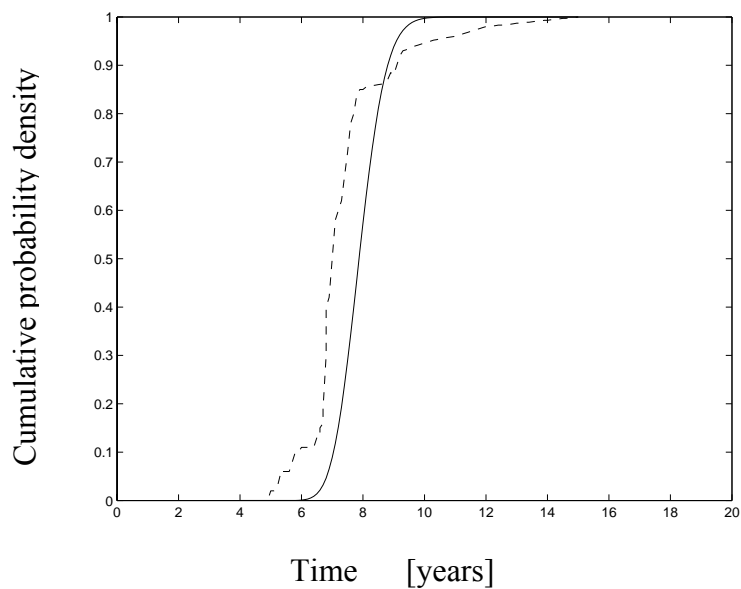
Fig. 7 *Example of cumulative residence time PDF showing a multi-peak behaviour. In the figure, the dashed line denotes the simulated g(τ) according to case SKI0/NF0/BC0 Run 6 Source 13 (Geier, 1996) and the solid line denotes the fitted 1-D model, where the values are x=500 m, u=63 m/y and E=120 m²/y.*

3.4 A comparison of the travel time approach and the one-dimensional continuum model

In this section, we compare the results of the 1-D continuum model mentioned in section 2.7 with the travel time approach proposed in this study. The study is focused on analysing the impact on the solute transport caused by translating 3-D description of the water flow into a 1-D description.

The approach proposed here convolutes the solution to the 1-D solute transport model water residence time PDF, $g(\tau)$, in Figs. 6 and 7 according to (1). The solute mass response function $f(t, \tau)$, is expressed according to the theory of section 2.2. The solution of (14) in real time domain was obtained by using a numerical inversion algorithm (De Hoog et al., 1982). The hydrological parameters associated with the macro-flow behaviour in the 3-D model are translated into a 1-D hydraulic dispersion coefficient, E, Darcy velocity, q, and a wet surface, a, and they are used in a 1-D continuum model for solute transport.

The coefficients and other parameter values used in the 1-D continuum model simulation given in Table 4 were used in SITE 94 (SKI, 1996). For instance, the k_d-value of 1 was applied to the scooping calculations representing a hypothetical stable radionuclide in the SITE 94 study. The same parameter values were used in the travel-time approach except the values of velocity and aperture that, in the 1-D approach are equivalent to the Darcy velocity, flow wetted surface area and matrix porosity. These values were derived from the simulations based on the discrete-feature network and taken as u=140 m/y and h=0.002 m.

Fig. 8 shows that there is a small difference between these two solutions when the 3-D water residence time PDF are taken according to Fig. 6. The relatively good agreement is expected, because the selected $g(\tau)$ has a close to Gaussian distribution. The implication is that $g(\tau)$ can be well represented by fitting up to the second temporal moment and the 1-D solute transport model (see section 2.7) is equipped to do this. The 1-D approach can represent the solute breakthrough curve up to the forth temporal moment (adapting parameters for advection, dispersion and limited matrix diffusion).

The main limitation of the 1-D approach lies in possibilities to account for complications of the water flow not considered in the basic formulation, i.e. irregularities

of the g(τ) not possible to represent up to the fourth temporal moments. One such common situation occurs due to multiple transport pathways for a given plume migration in the discrete fracture network. Fig. 7 shows a generic example of a residence time distribution (cumulative PDF) with a multi-peak behaviour of inert water parcels traveling through the network.

Fitting of 1-D advection-dispersion solution to a multi-path residence time PDF yields an estimate of velocity, u, which is intermediate to the advective velocities along both path, and an effective dispersivity which is much greater than along either path (Geier, 1996). The result is a clear bias of the fit as seen in Fig. 7 and this cannot be compensated in the solute transport analysis as seen in Fig. 9. Fig. 9 shows a significant difference between the simulated residence time PDF of reactive transport by using the 1-D continuum transport model and the travel time approach. As can be seen from Fig. 9 the multi-peak behaviour implies an early arriving of the fore-front of the breakthrough (a channelling effect).

In real fractured bedrock there is likely to be a multi-peak behaviour of the breakthrough due to the large amount of travel path possibilities in a fracture network. As mentioned, Fig. 7 shows such a multi-peak behaviour based on geological data taken for the SITE-94 application of the discrete-feature model. In Fig. 9 we can see a corresponding deviation between the 1-D approach and the travel time approach. This particular example has special importance for assessing the two approaches since all underlying data applies to a safety assessment exercise that generally is considered to have practical significance.

Table 4 *Parameter values for the simulations (SKI, 1996)*

Parameter	Value	Unit
Penetration depth into matrix, Z	0.1	m
Rock matrix porosity	1.0×10^{-3}	-
Flow porosity,	1.0×10^{-4}	-
Diffusion coefficient in porewater of the rock matrix, D_m	1.6×10^{-2}	m^2/year
Sorption coefficient, k_d	1	m^3/kg
Migration distance, X	100	m
Half-life time for a hypothetical stable nuclide	10^{38}	years
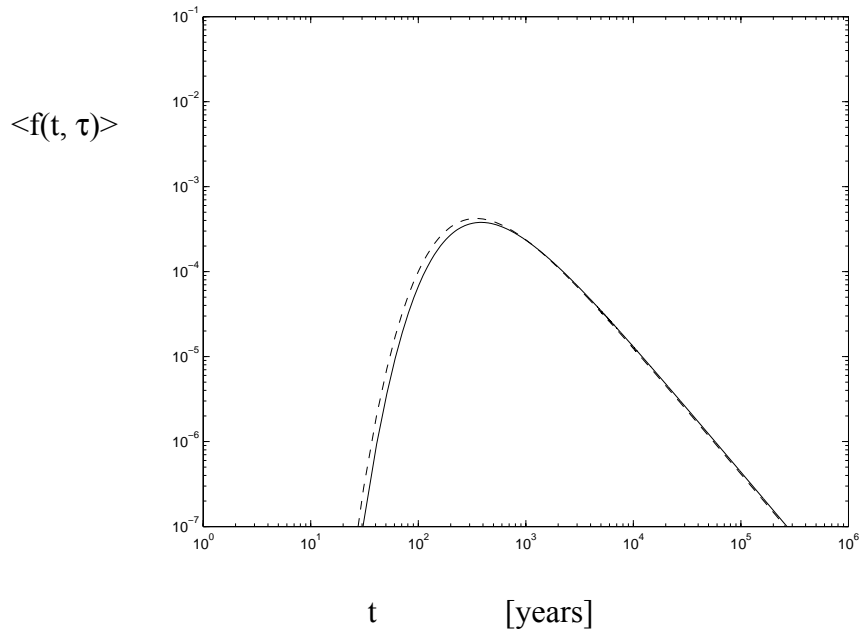
Fig. 8 *Comparison of the residence time PDF of sorbing solutes using the 1-D transport model solution (39) (dashed curve) and the travel time approach (1) in which f(t, τ) is expressed by (14) (solid curve). This graph shows a non-channelled case with a water residence time PDF according to Fig. 6.*
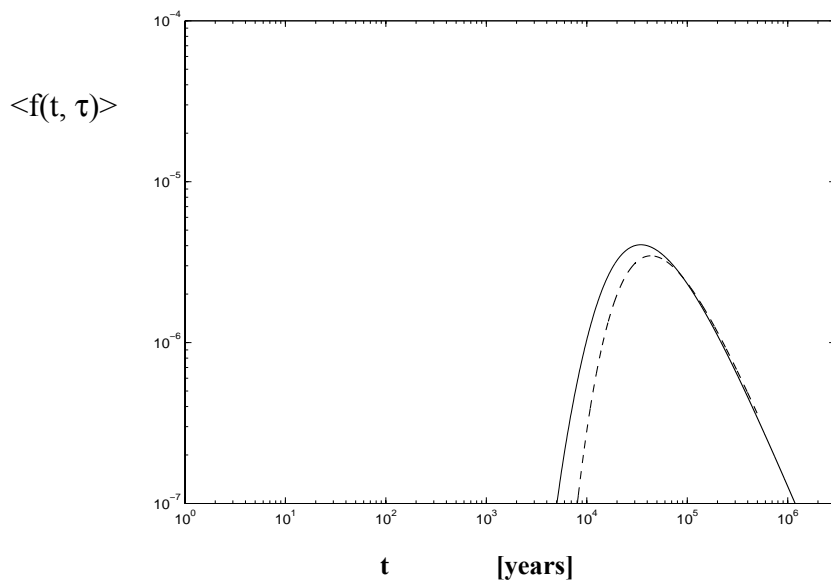
Fig. 9 *Comparison of the residence time PDF of sorbing solutes using the 1-D transport model solution (39) (dashed curve) and the travel time approach (1) in which f(t, τ) is expressed by (14) (solid curve). This graph shows a channelled case with a water residence time PDF according to Fig. 7.*

4. Determination of longitudinal dispersion coefficient on a fracture scale

The discrete-feature modelling is represented in terms of a set of interconnecting, transmissive, discrete features, each of which is essentially two-dimensional. A "discrete feature" in this context may represent a single conductive object (e.g. a single fracture) or a collection of objects that acts as a unit (e.g. a fracture zone). Since the whole modelling work is so complicated, each single fracture is constructed with constant aperture. The microscopic hydraulic effects in each single fracture are thus modelled by a longitudinal and a transversal dispersion coefficient, D_L and D_T, in a fracture scale as mentioned in section 3.2. In this chapter, we describe the basis for deriving those coefficients (section 4.1) and also provide results of a simulation study that demonstrates the relative importance of the microscopic dispersion due to shear dispersion.

4.1 Theoretical background

Taylor (1953) studied the spreading of dissolved solutes in laminar flow in a pipe caused by the wall shear and the associated velocity profile in the cross-section. The mechanism is known as "shear dispersion". A background is that inert particles (e.g. molecules) wander randomly throughout the cross-section of the pipe due to Brownian motion/molecular diffusion and would be affected by all the advective velocities present in the cross-section. This causes a spreading of the particles along the flow direction, which results in the microscopic dispersion we are discussing here. The microscopic dispersion can be modelled by means of a discrete random walk of the inert particles and be superimposed on the advective velocity profile (Bruderer and Bernabé, 2001).

The method used in this study to estimate the dispersion coefficient can be summarised in the following steps:
(1) Construct heterogeneous fields of the fracture aperture,
(2) solve the steady-state flow equation for the set of aperture fields,
(3) estimate the residence time PDF of inert particles travelling through the fractures using particle tracking, and
(4) estimate the longitudinal dispersion coefficient associated with the one-dimensional advection/diffusion equation.
These four steps are now explained more thoroughly:

1) A large number of spatially stochastic aperture fields were generated for different statistics by using HYDRO_GEN (Bellin and Rubin, 1996). The fracture statistics was taken from the findings of Hakami (1995), who collected drill cores with natural fractures from Äspö Hard Rock Laboratory, Sweden. She found that the coefficient of variation of the aperture increases significantly with the mean aperture in the studied intervals 0.1 mm <E[h]< 2 mm and 0.2<CV[h]<1.3, where E[…] denotes the operator of the expected value and CV[…] the operator of the coefficient of variance. The correlation length associated with the exponential covariance model was found to lie in the range 2 mm< ℓ <40 mm.

2) Fluid flow in a fracture of variable aperture is described by the cubic law (Moreno et al., 1988; Tsang and Tsang, 1989; Dverstorp et al., 1992; Cvetkovic et al., 1999):

$$\frac{\partial}{\partial x}\left(h^3(x,y)\frac{\partial p}{\partial x}\right) + \frac{\partial}{\partial y}\left(h^3(x,y)\frac{\partial p}{\partial y}\right) = 0 \tag{43}$$

where p is the pressure [Pa], h is the fracture aperture [m], and x and y are the Cartesian co-ordinates in the fracture plane.

The flow velocity vectors in the fracture are obtained by neglecting inertia effects (assuming uniform flow) and are given by $u = -\left((h/2)^2/2\mu\right)\left[(z/(h/2))^2 - 1/4\right]\nabla p$, where μ is the dynamic viscosity and z is the vertical co-ordinate from the central line (see Fig. 10). The velocity profile in each segment of the fracture, which has a certain aperture depth, h, is divided into 11 layers (Fig. 10). The mean velocity vector in the fracture is given by $u_{mean} = -\left((h/2)^2/12\mu\right)\nabla p$. The numerical code of Wörman and Xu (1996) is used to solve equation (43).

3) The streak-line field is computed by tracking a large number of inert particles travelling in the velocity field. The number and spatial distribution of the particles released at the upstream boundary are weighted according to the flow rate at the release point. The exact release point of each particle is randomly chosen. The molecular and shear dispersion are modelled in a similar way to that used by Bruderer and Bernabé (2001). The approach is described in the following.

At fixed time intervals, Δt, an inert particle will travel a fixed distance, $\Delta \xi$, in a random direction along the streak-line co-ordinate, ξ (move horizontally). The distance

travelled during each time interval is equated from $\Delta\xi = \sqrt{6\Delta t D_m}$ (Reif, 1965; Bruderer and Bernabé, 2001), where D_m is the molecular diffusion coefficient. Simultaneously, inert particles can jump randomly between layers with different velocities (move vertically). The velocity change for particles is assumed to be instantaneous, and the particle will have the velocity of the new layer after the jump. The simulation takes into account the reflection of particles from the ceiling or floor of the fracture walls.
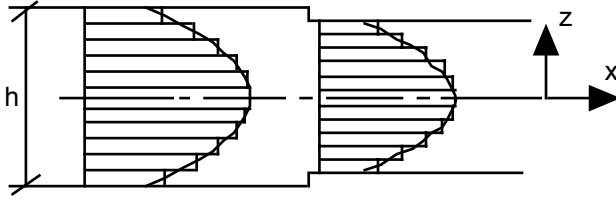
Fig. 10 *Schematic representation of the model of the microscopic dispersion as a result of a discrete random walk of the inert particles and superimposed on the advective velocity profile.*

The PDF of the residence time of inert particles is denoted $g(\tau)$, where τ is the travel time. By means of Monte Carlo simulations we can obtain the expected value of the PDF of the residence time of inert particles over an ensemble of fractures, $E[g(\tau)]$.

4) The longitudinal dispersion coefficients, D_L, associated with the one-dimensional advection/diffusion equation are estimated by using spatial moments of the above-mentioned PDF of the residence time of inert particles in the simulation fracture. The corresponding longitudinal dispersion coefficient is given by (Nordin and Troutman, 1980):

$$D_L = u_m^2 \sigma_t^2 / (2\mu_t) \tag{44}$$

where u_m is the mean velocity associated with the 1-D advection/diffusion equation corresponding to our simulated domain, σ_t^2 is the variance of the residence time and μ_t is the expected residence time.

4.2 Empirical relationship between dispersivity and Peclet number

Monte Carlo simulations with 500 realisations and totally over 500,000 particles were used to derive the expected value of the residence time of inert water parcels in a single fracture, where the combined effect of molecular diffusion and shear dispersion (Fig. 11) is taken into account. The coefficient of variation of the fracture aperture varied from 0.7 to 1. The simulation domain was $1{\times}1$ m^2. To eliminate the effects of longitudinal boundaries on the flow field, the particle tracking in each realisation was performed on a sufficiently small sub-domain within the whole simulation domain.

The variance of the residence time PDF, where molecular diffusion and shear dispersion are taken into account, is about 25% higher than if these microscopic dispersion effects are neglected. This result is due to the fact that the fracture dispersion is dominated by the variation in residence times for different flow paths, rather than the shear dispersion. Dispersion due to flow path distribution is primarily related to boundary conditions and aperture statistics, whereas shear dispersion is related to the Peclet number, $E[h]\,u_m/D_m$.

The ratio D_L/u_m, known as intrinsic dispersion coefficient or dispersivity, α_L [m], is often used to estimate the longitudinal dispersion coefficient (de Marsily, 1986). Fig. 12 shows α_L -values as a function of the Peclet number for various statistics of the heterogeneous aperture. The α_L-values lie in the range 0.16 to 0.52. The effect of shear dispersion is relatively small, which can be noticed as an insignificant change in the α_L-values for a change in the Peclet number. A change of the fracture aperture statistics has a larger impact on the flow field in the fracture and the overall dispersion behaviour. Since, the fracture is open on both the inlet and outlet boundary, the problem is essentially 1-D and the results in Fig. 12 apply to all fractures with such open boundaries regardless of size.
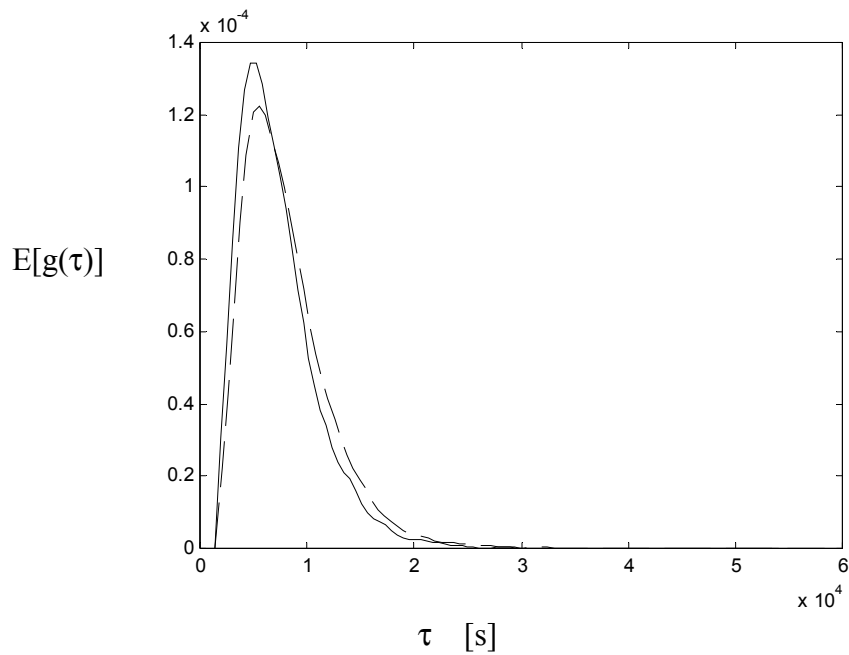
Fig. 11 *The ensemble average of the residence time PDF, E[g(τ)], in a 1-meter-long fracture with the aperture statistics E[h]=1.57 mm, CV[h]=1.0 and a correlation length of 0.06m, the dashed line represents the simulated result with molecular diffusion and shear dispersion taken into account and solid line represents the simulated result without molecular diffusion and shear dispersion taken into account.*
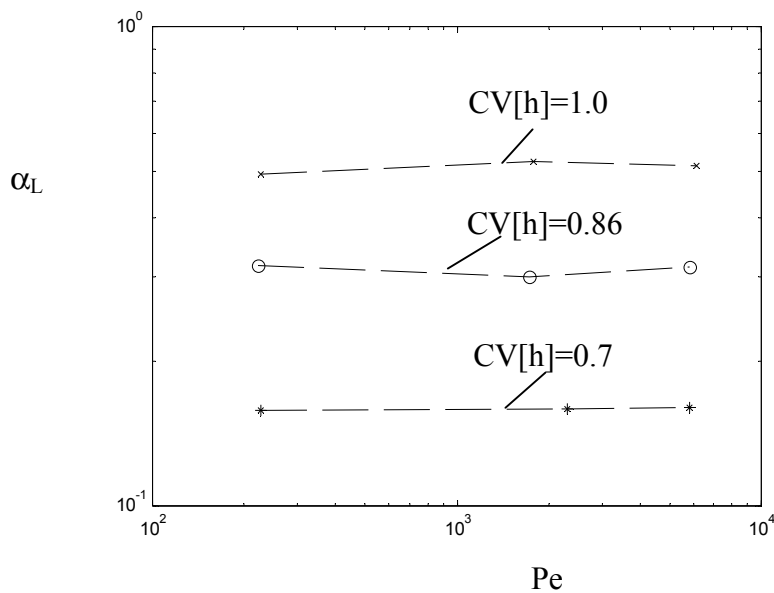
Fig. 12 α_L *versus the Peclet number for various statistics of the fracture aperture, in which* $Pe = E[h]u_m/D_m$ *and* $D_m = 1 \times 10^{-9}$ *m^2/s.*

5. Discussion of model behaviour based on site specific data

5.1 Uncertainty due to spatial variability of mass transfer

The importance of taking into account the uncertainty in heterogeneous rock properties for radionuclide migration was analysed and exemplified for plausible cases of radionuclides migrating from a waste repository in the Swedish granitic bedrock based on the data obtained from a single fracture (Wörman et al., 2003). We can extend that analysis to a network scale using (29) to (33) with the 26 terms instead of 7 terms in the covariance expression of the rock properties as discussed in section 2.6.

The empirical basis for such an extension is taken with respect to geology and geohydrology from the safety assessment exercise performed by the Swedish Regulatory (SKI, 1996) with the use of data from Äspö Hard Rock Laboratory. The flow analysis follows the approach described in section 3.2. Data on parameter variability on a fracture scale in the Äspö bedrock was taken from the studies of Xu and Wörman (1998) and Hakami (1995). The fracture scale parameters will be mentioned in some more detail after a brief discussion on the hydrological analysis and the statistical treatment of flow velocity and fracture aperture in the DF network model.

The size of the calculation domain over all is 5 km x 5 km x 1 km, but the stochastic DFN portion is a block 450 m x 320 m x 80 m. However, deterministic fracture zones pass through that block, so the domain crossed by the trajectories within the stochastic DFN portion of the model is smaller.

For simplicity in this example, only two pathways are investigated with respect to auto-covariance of flow velocity and fracture aperture, one relatively short pathway and one longer pathway. Both trajectories start at Canister Position 2 in SKI R 96:7 Fig 2.5. Although they start within 10 cm of each other, they exit the stochastic portion of the fracture network (referred to as the second feature type in section 3.1) and enter the deterministic fracture zones at points 11.5 m apart (referred to as the first feature type in section 3.1), which is an example of network dispersion. The statistics of the random fracture discs are given in Section 3.2.

Clearly, for both types of pathways (P.W.) there is a notable correlation length in both flow velocity and fracture aperture that is longer than the size of the fracture (Fig. 13).

For the short pathway, the coefficient of variance is 2.86 for velocity and 0.10 for aperture. For the
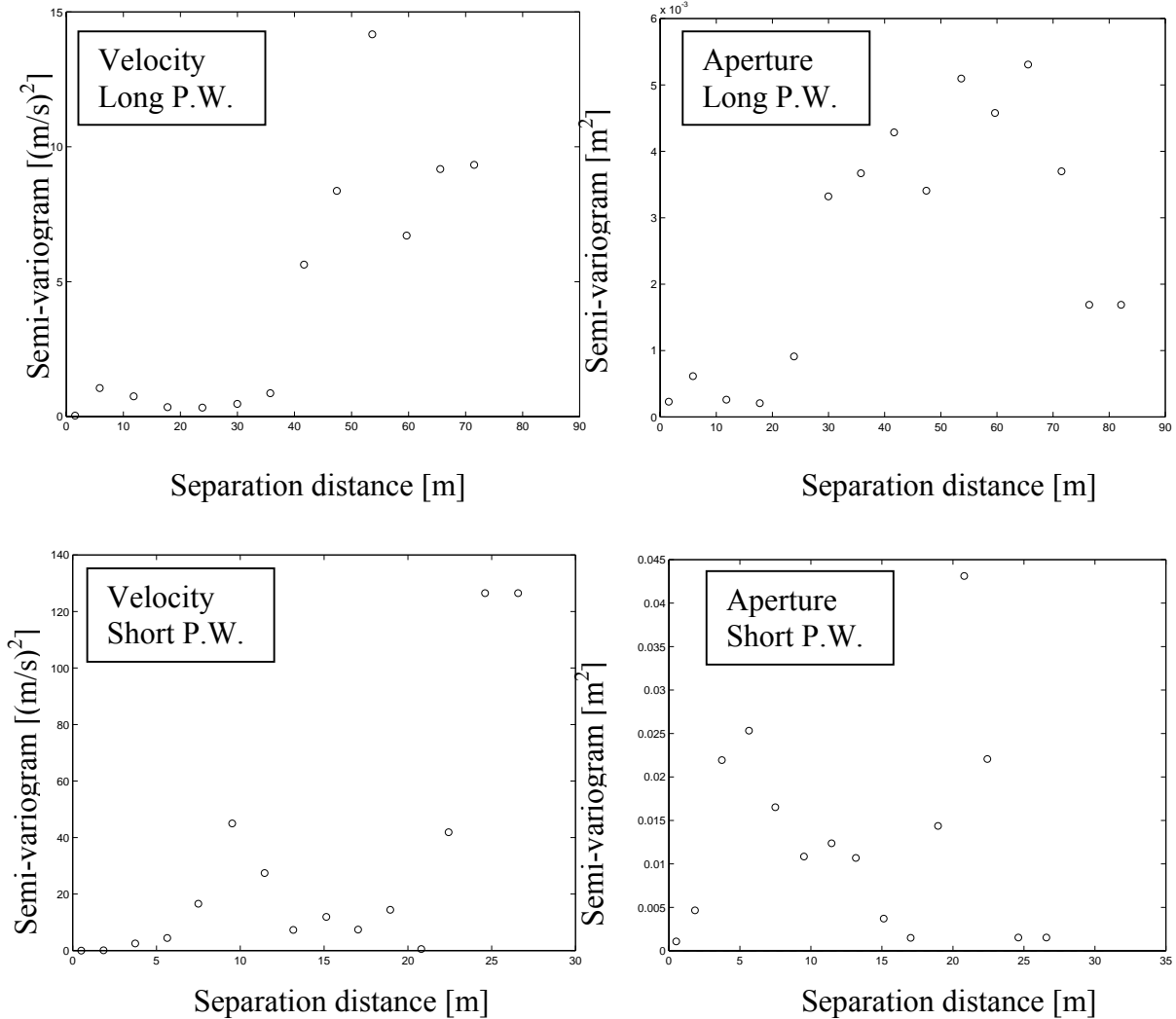
Fig. 13 *Semi-variogram of fracture aperture and flow velocity along two pathways in the discrete fracture fracture network that was used in the Site-94 study (SKI, 1996).*

long pathway, the coefficient of variance is 1.47 for velocity and 0.04 for aperture. The great difference is due to the cubic law for the flow (Tsang and Tsang, 1989). The approximate values on correlation length and variances that are used in the subsequent analysis are listed in Table 5.

The correlation structure of aperture and flow velocity is similar in that they exhibit the same correlation length and a similar cyclic behaviour. The exact result should depend

on the type of correlation structure used to generate the fracture network, but this result presented here is for a spatially non-correlated generation of fracture properties. Since the correlation structure found here extends beyond the individual fractures, the problem of generating a geostatistically representative fracture network properties is obviously important for the entire transport analysis.

Due to lack of data, the coefficient of variation and correlation length of rock matrix property, M'_n, is assumed to be 4 m. The coefficient of variation of rock sorption property, M, are assumed to be the same as that of the single fracture.

Geostatistics of the matrix property M, aperture and flow velocity for single fractures were obtained from Äspö crystalline rock in a one-meter scale (Xu and Wörman, 1998; Xu et al., 2001; Hakami, 1995). The statistics of the matrix property are obtained from direct measurements, whereas the velocity and aperture variation are evaluated along flow trajectories arising in Monte Carlo flow analyses with fractures with spatially variable aperture (Xu et al. 2001). The information of both statistics and parameter values are summarised in Table 5 and 7.

One analysis of the importance of accounting for the uncertainties in the bedrock properties is based on (29) and (30) with numerical inversion. In this way, we can study the expectation of the transport process and the confidence interval around the expectation. The other approach utilised herein is to use (31) and (33) to obtain the temporal moments of the PDF for the residence time of solute transport, which can be expressed in terms of expected value, variance, skewness as well as higher order moments of the residence time and are generally considered to be "effective" transport properties. This section describes a sensitivity analysis on the ratio of the variance and skewness of the residence time with and without account taken to heterogeneity of the rock properties, i.e. $\sigma_t^2 / \sigma_t^2(H_i = 0)$ and $S_t/S_t(b_i = \ell_i = 0)$.

First we make use of the temporal moments. To simplify the analysis, the effects of the actual (real) spatial parameter variability along the transport paths were omitted, i.e., all expected values of η were assumed to be unity. Further, for most radionuclides in crystalline rock 1<<R and if we assume an instantaneous sorption process equations, (32) and (33) can be simplified as

$$\frac{\sigma_t^2}{\sigma_t^2(H_i = 0)} \approx 1 + 3R\sum_{i=1}^{26} H_i \qquad (45)$$

$$\frac{S_t}{S_t(b_i = \ell_i = 0)} \approx 1 + \frac{5}{2}R\left[2\sum_{i=1}^{26} H_i + 3R\sum_{i=1}^{26}\left(H_i\frac{\ell_i}{uT}\right)\right] \qquad (46)$$

Table 5 *Geostatistics of parameters for single fracture and network.*

	Correlation length	Variance	References
<u>Single fracture</u> rock sorption property aperture flow velocity	$\ell_M = 0.1$ m $\ell_h = 0.18$ m $\ell_u = 0.18$ m	$\mathrm{Var}[\tilde{M}/M] = 0.3$ $\mathrm{Var}[\tilde{h}/h] = 0.7$ $\mathrm{Var}[\tilde{u}/u] = 0.14$	Xu and Wörman, 1998 Hakami, 1995 Xu et al., 2001
<u>Fracture network (SKI, 1996)</u> aperture flow velocity	$\ell_h = 10$ m $\ell_u = 10$ m	$\mathrm{Std}[\tilde{h}/h] = {\sim}0.1$ $\mathrm{Std}[\tilde{u}/u] = 2$	Tentative example based on the Site-94 study (SKI, 1996)
<u>Fracture network</u>	$\ell_M = 4$ m	$\mathrm{Var}[\tilde{M}/M] = 0.3$	Assumed

Given the statistics of Table 5, we can calculate the sum of $\ell_i b_i$ for single fracture and network scale to be 0.24 and 23, respectively, and the sum of $\ell_i^2 b_i$ for single fracture and network scale to be 0.03 and 211, respectively. In both estimations, we have ignored mixed terms between single fracture and network, such as $E^2[\eta_M]\mathrm{var}[\eta_{u,s}]\mathrm{var}[\eta_{h,n}]$ (see Table A3-1).

In this generic example, these mixed terms contributes to only 2% to the sum of the $\ell_i b_i$-term that is governing the impact of heterogeneity on the variance of the residence time PDF. Skewness depends also on the contribution to the $\ell_i^2 b_i$-term. The variation of the transport properties on the network scale accounts for 97% of the contribution to the $\ell_i^2 b_i$-term. The remaining percent is due to the variation in transport properties in single fractures. Terms reflecting variation of only one transport property (as distinct from

products of variances between two properties) stands for about 90% of the total contribution to the $\ell_i^2 b_i$-term.

Consequently, the larger correlation lengths characterising the heterogeneity of rock properties on the network scale imply that those variations on the network scale generally dominate the effect on the variance and skewness of the residence time. An exception can be found for the aperture of which its single fracture variation contributes with 0.53% to the $\ell_i^2 b_i$-term and its network variation contributes with 0.42% to the $\ell_i^2 b_i$-term. This is due to

Table 6 *Effect analyses of the heterogeneous matrix diffusion for different fracture aperture and sorption characteristics. The following parameter values apply: $\varepsilon/\varepsilon_t = 1$, $D_e = 10^{-13}$ m^2/s, $L = 0.05$ m, $\varepsilon = 0.004$, $\sum(\ell_i\ b_i) = 23$ and $\sum(\ell_i^2\ b_i) = 211$. Further, a rapid sorption is assumed; $k_r \rightarrow \infty$.*

h [m]	u [m/s]	u [m/year]	$2\dfrac{\varepsilon_t D_p}{huL}$	$\dfrac{\sigma_t^2}{\sigma_{t(H_i=0)}^2}$	$\dfrac{S_t}{S_t(\ell_i = b_i = 0)}$
1.00E-05	3.40E-09	1.07E-01	1.18E+02	8.12E+03	8.76E+09
3.00E-05	3.06E-08	9.65E-01	4.36E+00	3.02E+02	1.20E+07
9.00E-05	2.75E-07	8.69E+00	1.61E-01	1.21E+01	1.69E+04
2.70E-04	2.48E-06	7.82E+01	5.98E-03	1.41E+00	3.74E+02
6.44E-04	1.41E-05	4.45E+02	4.40E-04	1.03E+00	2.14E+00
2.43E-03	2.01E-04	6.33E+03	8.20E-06	1.00E+00	1.02E+00

the relatively small variance of the aperture encountered along the preferential flow paths on the network scale.

Generally, however, we can use only the geostatistics of rock properties for the network scale to analyse the effect of heterogeneity on solute transport. This means that the heterogeneity terms (H-terms) of the solutions (45) and (46) can be reduced from the 26 terms of Table A3-1 to 7 terms representing the geostatistics on the network scale.

Table 6 shows that the impact of the heterogeneity of the rock properties on the residence time PDF diminishes with increasing fracture aperture. Significant effects are obtained, however, for fracture apertures smaller than a few tenths of a millimetre for the conditions prevailing in the Swedish granitic bedrock. Particularly large deviations arise in the skewness between the homogeneous and the heterogeneous cases. The variances and

the correlation lengths of $\tilde{u}$, $\tilde{h}$ and $\tilde{M}$, respectively, have the same effect on the residence time PDF, as is clear from (45) and (46). However, based on the specific statistic used here, the terms of H_i that reflect heterogeneity of the rock property $\tilde{M}$ contributes to about 10% of the

total sum of H_i. Heterogeneity of $\tilde{u}$ and $\tilde{h}$ contributes to 20% of the total effect of the heterogeneous rock properties on the variance of the travel time PDF respectively. Heterogeneity of $\tilde{M}$, $\tilde{u}$ and $\tilde{h}$ jointly contributes to the remaining 50%.

As an example we apply Eq. (30) on ^{137}Cs to quantify the uncertainty in predictions of solute transport. The variance of c' is found by means of the Laplace inversion of (30) using the numerical method of De Hoog (1982) and evaluating the expectation E[c'c']. Fig. 14 shows both the expected accumulated mass <M> normalized by the total mass M_0 and confidence intervals defined in terms of $\pm\sigma_M/M_0$, in which $M_0 = \int_0^\infty c(x,t)dt$. The parameter values used in the simulation are specified in Table 7. There are significant uncertainties about the expectation of the transport problem as can be concluded from the figure. The time corresponding ton 50% mass recovery falls within the prediction interval $10^4 - 10^5$ years and, in this interval, there is an uncertainty about timing of about one order of magnitude due to the uncertainty of the rock properties.

Table 7 *Parameter values used in estimation of the uncertainty in predictions of solute transport.*

$\ell_M = 4$	[m]		$D_e = 10^{-13}$	[m^2/s]
$\ell_h = 10$	[m]		$D_p = 10^{-10}$	[m^2/s]
$\ell_u = 10$	[m]		$\varepsilon = 0.004$	[-]
Var[$\tilde{M}/M$]= 0.3	[-]		$k_d = 0.008$	[m^3/kg]
			$k_r = 10\text{-}10$	[1/s]
Var[$\tilde{h}/h$] = 0.1	[-]		$x = 500$	[m]
			$h = 0.0064$	[m]
Var[$\tilde{u}/u$]= 2	[-]		$u = 50$	[m/y]
			$L = 0.1$	[m]
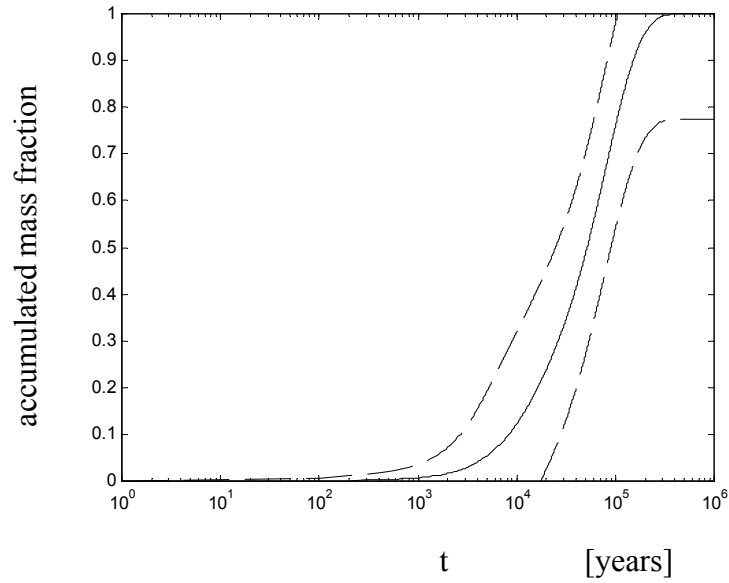
Fig. 14 *Accumulated solute mass resulting from a pulse of a reactive solute traveling through a fracture network, in which the solid line denotes the expected cumulative breakthrough curve (BTC), the dash lines denote plus/minus one standard deviation.*

5.2 Combination of flow effects and uncertainty of spatial variability of mass transfer

Until now we have shown how to obtain the water residence time PDF, $g(\tau)$, in a discrete fracture network and the response function, $f(t)$, for radionuclides accounting for the uncertainty of spatial variability in bedrock properties. Effects of uncertainty of the heterogeneous rock property on radionuclide transport in three dimensions can be analysed by using the travel time approach Eq. (1). By means of Laplace transforms (Xu et. al., 2001) we obtain the temporal moments for the multi-dimensional case as

$$< m_j >= \int_0^\infty (-1)^j \left. \frac{\partial^j \bar{f}(p,\tau)}{\partial p^j} \right|_{p=0} g(\tau)d\tau = \int_0^\infty m_j(\tau)g(\tau)d\tau \qquad (47)$$

The variance of the residence time PDF can be obtained from $\left. \sigma_t^2 \right|_{MD} = <m_2> - [<m_1>]^2$, in which subscript 'MD' denotes multi-dimensional (two or three). Higher order central temporal moments can be expressed similarly. Because the moments $(31) - (33)$ are

52

linear functions of the integrand $\tau = x/u$, contained in (47), the temporal moments associated with the one- and two-dimensional cases will follow the same function of the rock properties if the properties are independent of τ. For such conditions we get

$$< m_j(\tau) >= m_j(< \tau >) \tag{48}$$

in which j=1,2,3. The consequence is that the expressions for the central temporal moments (i.e. (31) – (33))) form a suitable basis also in multi-dimensional flows for analysis of the effect of the heterogeneity in rock properties on the solute transport up to the third central temporal moment. More precisely, $\mu_t|_{MD} = \mu_t(< \tau >)$, $\sigma_t^2|_{MD} = \sigma_t^2(< \tau >)$ and $S_t|_{MD} = S_t(< \tau >)$. As shown in section 3.3, in many cases a reasonable approximation of the residence time PDF of inert water parcels in fractures is an exponential function of the form $g(\tau) = \lambda \exp[- \lambda (\tau - \tau_1)]$; $\tau \in [\tau_1, \infty]$ and $g(\tau) = 0$; $\tau \notin [\tau_1, \infty]$, in which λ is a constant . The mean value of the water residence time can be expressed as $<\tau>/\tau_1 = 1 + 1/(\tau_1 \lambda)$, where $(\tau_1 \lambda)$ was found to be about 1 for the investigated fractures. In the case of $\lambda \to \infty$ we get the "plug flow case" $g(\tau) = \delta(\tau_1)$, where $\delta(\tau)$ is the Dirac Delta function. If, as an option to (48), the fracture averaged moment $<m_j>$ is instead normalised with $m_j(\tau_1)$ we get $<m_j> = [1 + 1/(\tau_1 \lambda)] m_j(\tau_1)$, which confirms the obvious result that channelled flow unconditionally enlarges the temporal moments compared to plug flow. In other words the effect of macrodispersion on the flow in a heterogeneous aperture network reduces the peak value of the breakthrough curve (solute concentration versus time relationship).

The preceding result is based on the assumption that the mean residence time of the flow is the same regardless of macro-dispersion. In a channelled flow, however, one essential effect is occurrence of fast pathways. To analyse such channelling effects and the importance of uncertainty of the heterogeneous rock properties on leakage of radionuclide from the repository to the biosphere, a fully three-dimensional flow analyses should be performed as described in section 3.3. The channelling effect in the network may lead to a much faster transport path for radionuclide migration.

6. Conclusions

This report shows how the heterogeneity in the bedrock properties has two fundamentally different implications for an analysis of radionuclide transport in saturated rock fractures. Firstly, the actual variation of bedrock properties causes migrating nuclides to encounter a certain (known) distribution of properties along their transport path. A second effect is due to the uncertainty about the statistical representativity of properties along an individual transport path, which is related to the discrete measuring technique. This uncertainty of what bedrock properties will actually be encountered along a transport pathway can, generally, be considered to be the main effect of the heterogeneity.

Closed form solutions of the central temporal moments of the residence time PDF are derived using exponential auto-covariance functions (equations (31)-(33)) that are found to apply to data obtained from bedrock samples taken at Äspö Hard Rock Laboratory, Sweden. The solutions are valid for both a single fracture and a network scale. The auto-covariances are represented individually for the advection velocity in the fracture, the fracture aperture and a typical matrix property including the effective diffusivity and the sorption distribution coefficient. The definition of both the typical matrix property and the exponential covariance functions most likely can be generalised to several rock types. Because the solution procedure involves spectral analysis, only the auto-covariance (and mean value) needs to be defined for the rock properties (e.g. not the type of distribution) in terms of exponential functions.

The auto-covariance is also separated in terms of local variations, within individual fractures, and regional/global variations of the in a network of fractures. Analyses based on geological data from Äspö, Sweden, indicate that the regional/global variation of flow velocity and fracture aperture dominates the effect on the solute transport over the local variation due to the longer correlation lengths. Probably, the same would apply to variation in rock matrix properties, but absence of relevant data prohibited such an analysis.

Hence, to be able to analyse the effect of flow and uncertainty in heterogeneous rock properties on performance assessments, large-scale variability in bedrock properties should be specifically accounted for. For definite conclusions on the relative importance of local- and regional-scale variabilities, site-specific data is needed on both a fracture-scale and for the bedrock as a whole.

A sensitivity analysis, performed with data typical to the Swedish crystalline bedrock, indicates that the effect of heterogeneous rock properties on the transport of radionuclides in rock fractures can be significant. Heterogeneity of the rock properties contributes to decreasing the peak value of a pulse travelling in a fracture and increasing the time of duration under which a certain dose is exceeded. The maximum variance of the solution increases with increasing variance of the rock properties and reduces with increasing correlation length of the properties.

The effect of the heterogeneity in the rock properties increases markedly with decreasing fracture aperture and the co-varying advection velocity (Table 6). Based on data valid for Äspö Hard Rock Laboratory in Sweden, significant effects of fracture-scale heterogeneous rock properties on expected values of radionuclide transport can be expected in fractures apertures smaller than about $200 - 300$ µm. The effect of variation of bedrock properties on the network-scale is probably much larger, which has great importance for implementation in for instance risk assessments. In a specific example of a network-scale problem (Fig. 14), accounted for in the report, the time corresponding to 50% mass recovery could be predicted only within a confidence interval (based on ± one standard deviation) of one order of magnitude.

By applying the travel time approach (the Lagrangian method of description), the transport problem in a multi-dimensional fracture can be decomposed into a multi-dimensional flow problem and a one-dimensional mass transfer problem. We demonstrate from convolution principles how the complete multi-dimensional solution, in terms of temporal moments of the residence time PDF, is obtained by substituting the travel time for the individual path with an arithmetic mean for all paths (cf. equation (48)). If the flow residence time PDF is close to Gaussian, the travel time and 1-D continuum approach give almost the same result (Fig. 8). This is because the 1-D approach can well represent the Gaussian function. However, if there is a multiple-peak flow residence time PDF or in another way more erratic flow response on the network scale, the travel time approach is superior to the 1-D transport modeling. Examples taken from SITE 94 study showed that such cases can be found in safety assessments based on site data..

7. References

Andersson, J. and Dverstorp, B., 1987. Conditional Simulations of Fluid Flow in Three-dimensional Networks of Discrete Fractures, Water Resource Res., 23(10), 1876-1886.

Bellin, A. and Rubin, Y. (1996). HYGRO_GEN: A Spatially Distributed Random Field Generator for Correlated Properties. Stochastic Hydrology and Hydraulics. 10, 253-278.

Bruderer, C. and Bernabé, Y. (2001). Network Modeling of Dispersion: Transition from Taylor Dispersion in Homogeneous Networks to Mechanical Dispersion in Very Heterogeneous Ones. Water Resour. Res., 37(4), 897-908.

Cvetkovic, V., Selroos, J. O. and Cheng, H., 1999. Transport of Reactive Tracers in Rock Fractures. J. Fluid Mech. 378, 335-356.

Cvetkovic, V., Selroos, J.-O., 1999. Geosphere Performance Indices: Comparative Measures for Site Selection and Safety Assessment of Deep Waste Repositories, SKB-Report R-99-01, ISSN 1402-3091.

Dagan, G, 1989. Flow and Transport in Porous Formations, Springer-Verlag, Berlin.

De Hoog, F.R., Knight, J.H., Stokes, A.N., 1982. An Improved Method for Numerical Inversion of Laplace Transforms, J. Sci. Stat. Comput., 3(3), 357-366.

Dverstorp, B., Andersson, J. and Nordqvist, W., 1992. Discrete Fracture Network Interpretation of Field Tracer Migration in Sparsely Fractured Rock. Water Resource Res., 28(9), 2327-2343.

Espinoza, C., Valocchi, A.J., 1997, Stochastic Analysis of One-dimensional Transport of Kinetically Adsorbing Solutes in Chemically Heterogeneous Aquifers, Water Resources Res., 33(11), 2429-2445.

Geier, J.E. (1996). Discrete-Fracture Modelling of Äspö Site: 3. Predictions of Hydrogeological Parameters for Performance Assessment. (SITE-94) SKI Report 96:7. Swedish Nuclear Power Inspectorate, Stockholm, Sweden.

Geier et al. (1992) Discrete-fracture network modelling, Finnsjön, Phase 2, SKB Technical Report 92-0x.

Geier, J., (2003). "Discrete-Feature Model for Flow and Transport in Fractured Crystalline
Rock: DFM Code Version 1.0 Technical Description and User
Documentation," SKI Report 03:xx.

Gelhar, L. W., Ko, P. Y., Kwai, H. H. and Wilson, J. L., 1974. Stochastic Modelling
of Groundwater System, Rep. 189, R. M. Parsons Lab. for Water Resour. and
Hydrodyn., Mass. Inst. of Technol., Cambridge.

Gelhar, L.W., Axness, C.L., 1983, Three-dimensional Stochastic Analysis of
Macrodispersion in Aquifers, Water Resources Res., 19(1), 161-180.

Grisak, G.E. and Pickens, J.F., 1980. Solute Transport Through Fractured Media: 1.
The Effect of Matrix Diffusion. Water Resources Res., 16(4), 719-730.

Gutjahr, A. L. Gelhar, L. W., Bakr, A. A. and MacMillan, J. R., 1978. Stochastic
Analysis of Spatial Variability in Subsurface Flows, 2. Evaluation and
Application. Water Resources Res. 14(5), 953-959.

Hakami, E., 1995. Aperture Distribution of Rock Fractures. Doctoral Thesis.
Department of Civil and Environmental Engineering, Royal Institute of
Technology, Stockholm.

Hakami, E., Barton, N., 1990, Aperture Measurements and Flow Experiments Using
Transparent Replicas of Rock Joints, Proc. Int. Symp. Rock Joints, Loen,
Norway, Eds. Barton and Stephansson, Balkema, Rotterdam, The
Netherlands,
383-390.

Hollenbeck, K. J., 1998. INVLAP.M: A Matlab Function for Numerical Inversion of
Laplace Transforms by the De Hoog Algorithm,
http://www.isva.dtu.dk/staff/karl/invlap.htm

Johansson, H., 2000. "Retardation of tracers in crytalline rock: Sorption and matrix diffusion
of alkali metal and alkaline earth metal tracers in laboratory and field
experments". Doctoral thesis. Chalmers University of Technology, Götborg,
Sweden, ISBN 91-7197-893-3.

Long, J.C.S. (1984) Ph.D thesis (or reference Long & Witherspoon WRR paper).

Lumley, J.L., Panofsky, H.A., 1964. The Structure of Atmospheric Turbulence, John
Wiley & Sons, New York.

Maloszewski, P. and Zuber, A., 1990. Mathematical modeling of tracer behaviour

in short-term experiments in fissured rocks. Water Resources Res. 26(7), 1517-1528.

Marsily, G. 1986. Quantitative Hydrogeology — Groundwater Hydrology for Engineers. Academic Press.

Moreno, L., Tsang, Y. W., Tsang, C. F., Hale, F. V. and Neretnieks, I. (1988). Flow and Tracer Transport in a Single Fracture: A Stochastic Model and Its Relation to Some Field Observations. Water Resour. Res. 24(12), 2033-2048.

Neretnieks, I., 1980. Diffusion in the Rock Matrix: An important factor in radionuclide retardation?, Journal of Geophysical Research, 85, 4379-4397.

Neuman,S. P., (1987). Stochastic Continuum Representation of Fractured Rock Permeability as an Alternative to REV and Fractured Network Concepts. Proc. 28th Symp. Rock Mech. Tucson, Arizona, edited by I. W. Farmer, J. J. K. Daeman. C. S. Desai, C. E. Glass, and S. P. Neuman, 533-561.

Nordin, C. F. and Troutman, B. T. (1980). Longitudinal Dispersion in Rivers: The Persistence of Skewness in Observed Data. Water Resour. Res. 16(1), 123-128.

Painter, S. and Cvetkovic, V. (2001). Stochastic Analysis of Early Tracer Arrival in a Segmented Fracture Pathway. Water Resour. Res., 37(6), 1669-1680.

Reif, F. (1965). Fundamentals of Statistical and Thermal Physics, 651 pp., McGraw-Hill, New York.

Rodriguez-Iturbe, I., Rinaldo, A., 1997, Fractal River Basins, Cambridge University Press, Cambridge, United Kingdom.

Schwartz, F. W. and Smith, L., 1988. A Continuum Approach for Modeling Mass Transport in Fractured Media. Water Resource Res., 24(8), 1360-1372.

Siitari-Kauppi, M., Lindberg, A., Hellmuth, K. H.,Timonen, J., Väätäinen, K., Hartikainen, J. and Hartikainen, K., 1997. The Effect of Microscale Pore Structure on Matrix Diffusion æ a Site-specific Study on Tonalite. J. Contaminant Hydrology, 26, 147-158.

SKI. 1996. SKI SITE-94. Deep Repository Performance Assessment Project. SKI Report 96:36. Swedish Nuclear Power Inspectorate, Stockholm, Sweden.

Taylor, G. (1953). Dispersion of Solute Matter in Solvent Flowing Slowly through a Tube, Proc. R. Soc. London, Ser. A. 219, 186-203.

Tsang, Y.W., Tsang, C.F., 1989. Flow Channeling in a Single Fracture as a Two-Dimensional Strongly Heterogeneous Permeable Medium, Water Resources Res., 25(9), 2076-2080.

Vanmarcke, E., 1988. Random Fields, The MIT Press, USA.

Wels, C. and Smith, L., 1994. Retardation of Sorbing Solutes in Fractured Media. Water Resources Res. 30(9), 2547-2563.

Wörman, A., Xu. S., 1996. "Simulation of Radio Nuclide Migration in Crystalline Rock under Influnce of Matrix Diffusion and Sorption Kinetics", Technical Report 96:22, Swedish Nuclear Power Inspectorate, ISSN 1104-1374.

Wörman, A., Xu, S. and Dverstorp, B. (2003). Kinematic Analysis of Solute Mass Flows in Rock Fractures with Spatially Random Parameters. Journal of Contaminant Hydrology, 60: 2003, 163-191.

Xu, S., Wörman, A., 1999. Implications of Sorption Kinetics to Radionuclide Migration in Fractured Rock, Water Resources Research, 35(11), 3429-3440.

Xu, S., Wörman, A., 1998. Statistical Patterns of Geochemistry in Crystalline Rock and Effect of Sorption Kinetics on Radionuclide Migration, SKI Report 98:41, Stockholm, Sweden, ISSN 1104-1374.

Xu, S., Wörman, A., Dverstorp, B., 2001. "heterogeneous matrix diffusion in crystalline rock – Implications for geosphere retardation of migrating radionuclides", Journal of Contaminant Hydrology, , FEB 2001: 47(2-4) 365-378.

Appendix 1: Derivation of cross co-variance function

The stochastic auxiliary variable, ´, can be defined in terms of a Fourier-Stiltjes integral (Lumley and Panofsky, 1964; Gelhar et al., 1974);

$$\beta' = \int_{-\infty}^{+\infty} e^{i\omega x} Z_{\beta'}(d\omega) \tag{A1-1}$$

in which Z is a complex stochastic amplitude with zero mean value given as a function of a small increment of the angular frequency, $d\omega$. Hence, if the spectral density of β' is defined as

$$\varphi_{\beta}(\omega) = \frac{E\left[Z_{\beta'}(d\omega)Z_{\beta'}^{*}(d\omega)\right]}{d\omega} \tag{A1-2}$$

we can readily show that the auto-covariance of β' is given by the inverse Fourier transform of $\varphi_{\beta'}$, in which the asterisk denotes the complex conjugate (Vanmarcke, 1988, 84-92). Similarly, if the cross-spectral density function is defined as

$$\varphi_{\bar{c}'\beta'}(\omega) = \frac{E\left[Z_{\bar{c}'}(d\omega)Z_{\beta'}^{*}(d\omega)\right]}{d\omega} \tag{A1-3}$$

the cross-covariance between β' and $\bar{c}'$ is given by the inverse Fourier transform of $\varphi_{c'\beta'}$.

Consequently, if the stochastic processes in (28), β' and $\bar{c}'$, are defined in terms of Fourier-Stiltjes integrals and the last two terms of (28) are omitted we obtain

$$i\omega Z_{\bar{c}'}(d\omega) + E\left[\tilde{\beta}\right]Z_{\bar{c}'}(d\omega) + E\left[\bar{c}\right]Z_{\beta'}(d\omega) = 0 \tag{A1-4}$$

Using (A1-3), the cross-spectrum of β' and $\bar{c}'$ becomes

$$\varphi_{\bar{c}'\beta'}(\omega) = -\frac{E[\bar{c}]}{E[\tilde{\beta}] + i\omega} \varphi_{\beta'}(\omega) \qquad (A1\text{-}5)$$

This expression relates the auto-spectrum of β′ to the cross-spectrum of c̄′ and β′. The cross-covariance can be obtained by means of convolution. We may write

$$Cov[\beta'(x+s)\bar{c}'(x)] = F^{-1}\left[-\frac{E[\bar{c}]}{E[\tilde{\beta}] + i\omega}\right] * F^{-1}[\varphi_{\beta'}] \qquad (A1\text{-}6)$$

in which F^{-1}[...] denotes the Fourier inversion and * is the convolution operator. The first term on the right-hand side of (A1-6) can be inverted by means of standard transforms and the inversion can be written as in (29).

Appendix 2: Auto-covariance of Auxiliary Variable $\beta(p; s)$

By using the simple approach, (21), we can express β in terms of perturbations, $\eta = E[\eta] + \eta'$ and $\tilde{\beta} = E[\tilde{\beta}] + \beta'$:

$$\tilde{\beta} = c_1 E[\eta_u] + c_1 \eta_u' + c_2 E[\eta_u] E[\eta_h] E[\eta_M] + c_2 E[\eta_u] E[\eta_M] \eta_h' + c_2 E[\eta_u] E[\eta_h] \eta_M' +$$
$$+ c_2 E[\eta_M] E[\eta_h] \eta_u' + c_2 E[\eta_M] \eta_u' \eta_h' + c_2 E[\eta_h] \eta_u' \eta_M' + c_2 E[\eta_u] \eta_M' \eta_h' + c_2 \eta_u' \eta_M' \eta_h'$$

(A2-1)

Hence,

$$E[\beta] = c_1 E[\eta_u] + c_2 E[\eta_u] E[\eta_h] E[\eta_M] + c_2 E[\eta_u] Cov[\eta_M \eta_h] + c_2 E[\eta_M] Cov[\eta_u \eta_h] +$$
$$+ c_2 E[\eta_h] Cov[\eta_u \eta_M] + c_2 Cov[\eta_u \eta_h \eta_M]$$

(A2-2)

Subtracting (A2-2) from (A2-1) yields

$$\beta' = c_1 \eta_u' + c_2 E[\eta_u] E[\eta_M] \eta_h' + c_2 E[\eta_u] E[\eta_h] \eta_M' + c_2 E[\eta_M] E[\eta_h] \eta_u' + c_2 E[\eta_u] \eta_M' \eta_h' +$$
$$+ c_2 E[\eta_M] \eta_u' \eta_n' + c_2 E[\eta_u] \eta_u' \eta_M' + c_2 \eta_u' \eta_M' \eta_h' - c_2 E[\eta_u] Cov[\eta_M \eta_h] - c_2 E[\eta_M] Cov[\eta_u \eta_h]$$
$$- c_2 E[\eta_h] Cov[\eta_u \eta_M] - c_2 Cov[\eta_u \eta_h \eta_M]$$

(A2-3)

By using $Cov[\beta'(x), \beta'(x+s)] = E\left[\left. \left(\tilde{\beta} - E[\tilde{\beta}] \right) \right|_x \left. \left(\tilde{\beta} - E[\tilde{\beta}] \right) \right|_{x+s} \right] = E[\beta_x' \beta_{x+s}']$ the auto-covariance β can be expressed

$$Cov[\beta'(s)] = \left(c_1^2 + E^2[\eta_h] E^2[\eta_M] c_2^2 \right) Cov[\eta_u(s)] + c_2^2 E^2[\eta_u] E^2[\eta_M] Cov[\eta_h(s)] +$$
$$+ c_2^2 E^2[\eta_u] E^2[\eta_h] Cov[\eta_M(s)] + c_2^2 E^2[\eta_u] Cov[\eta_h(s)] Cov[\eta_M(s)] +$$
$$+ c_2^2 E^2[\eta_h] Cov[\eta_u(s)] Cov[\eta_M(s)] + c_2^2 E^2[\eta_M] Cov[\eta_u(s)] Cov[\eta_h(s)] +$$
$$+ c_2^2 Cov[\eta_u(s)] Cov[\eta_h(s)] Cov[\eta_M(s)] + CC_1$$

(A2-4)

in which CC_1 represents several cross-covariance terms between the perturbations of different η's that are omitted in this study and c_1 and c_2 are coefficients that contain the Laplace variable p and defined in Table 1.

Appendix 3: Derivation of Auto-covariance of Auxiliary Variable β(p; s) in Network Scale

The covariance of β' which is expressed by (36) can be given as

$$Cov[\beta'(s)] = Cov\left[(\beta'_n + \beta'_s)_x (\beta'_n + \beta'_s)_{x+s}\right]$$

$$= Cov\left[\beta'_{n,x}\beta'_{n,x+s} + \beta'_{n,x}\beta'_{s,x+s} + \beta'_{s,x}\beta'_{n,x+s} + \beta'_{s,x}\beta'_{s,x+s}\right] \tag{A3-1}$$

If we neglect the cross covariance, $Cov[\beta'_{n,x}\beta'_{s,x+s}]$ and $Cov[\beta'_{s,x}\beta'_{n,x+s}]$ we have

$$Cov[\beta'(s)] = \left(c_1^2 + E^2[\eta_h]E^2[\eta_M]c_2^2\right)\left(Cov[\eta'_{u,s}(s)] + Cov[\eta'_{u,n}(s)]\right) +$$

$$+ c_2^2 E^2[\eta_u]E^2[\eta_M]\left(Cov[\eta'_{h,s}(s)] + Cov[\eta'_{h,n}(s)]\right) +$$

$$+ c_2^2 E^2[\eta_u]E^2[\eta_h]\left(Cov[\eta'_{M,s}(s)] + Cov[\eta'_{M,n}(s)]\right) +$$

$$+ c_2^2 E^2[\eta_u]\left(Cov[\eta'_{h,s}(s)]Cov[\eta'_{M,s}(s)] + Cov[\eta'_{h,s}(s)]Cov[\eta'_{M,n}(s)] +\right.$$

$$\left. + Cov[\eta'_{h,n}(s)]Cov[\eta'_{M,s}(s)] + Cov[\eta'_{h,n}(s)]Cov[\eta'_{M,n}(s)]\right) +$$

$$+ c_2^2 E^2[\eta_h]\left(Cov[\eta'_{u,s}(s)]Cov[\eta'_{M,s}(s)] + Cov[\eta'_{u,s}(s)]Cov[\eta'_{M,n}(s)] +\right.$$

$$\left. + Cov[\eta'_{u,n}(s)]Cov[\eta'_{M,s}(s)] + Cov[\eta'_{u,n}(s)]Cov[\eta'_{M,n}(s)]\right) +$$

$$+ c_2^2 E^2[\eta_M]\left(Cov[\eta'_{u,s}(s)]Cov[\eta'_{h,s}(s)] + Cov[\eta'_{u,s}(s)]Cov[\eta'_{h,n}(s)] +\right.$$

$$\left. + Cov[\eta'_{u,n}(s)]Cov[\eta'_{h,s}(s)] + Cov[\eta'_{u,n}(s)]Cov[\eta'_{h,n}(s)]\right) +$$

$$+ c_2^2\left(Cov[\eta'_{u,s}(s)]Cov[\eta'_{h,s}(s)]Cov[\eta'_{M,s}(s)] + Cov[\eta'_{u,s}(s)]Cov[\eta'_{h,n}(s)]Cov[\eta'_{M,s}(s)] +\right.$$

$$+ Cov[\eta'_{u,s}(s)]Cov[\eta'_{h,s}(s)]Cov[\eta'_{M,n}(s)] + Cov[\eta'_{u,s}(s)]Cov[\eta'_{h,n}(s)]Cov[\eta'_{M,n}(s)] +$$

$$+ Cov[\eta'_{u,n}(s)]Cov[\eta'_{h,s}(s)]Cov[\eta'_{M,s}(s)] + Cov[\eta'_{u,n}(s)]Cov[\eta'_{h,n}(s)]Cov[\eta'_{M,s}(s)] +$$

$$\left. + Cov[\eta'_{u,n}(s)]Cov[\eta'_{h,s}(s)]Cov[\eta'_{M,n}(s)] + Cov[\eta'_{u,n}(s)]Cov[\eta'_{h,n}(s)]Cov[\eta'_{M,n}(s)]\right) + CC_1$$

$$\tag{A3-2}$$

Table A3-1 *Definition of typical coefficients in Eqs. (33), (34) and (35).*

i	a_i	b_i	ℓ_i
1	$\left(c_1^2 + E^2\!\left[\eta_h\right]E^2\!\left[\eta_M\right]c_2^2\right)b_1$	$\mathrm{var}\!\left[\eta_{u,s}\right]$	$\ell_{u,s}$
2	$\left(c_1^2 + E^2\!\left[\eta_h\right]E^2\!\left[\eta_M\right]c_2^2\right)b_2$	$\mathrm{var}\!\left[\eta_{u,n}\right]$	$\ell_{u,n}$
3	$c_2^2 b_3$	$E^2\!\left[\eta_u\right]E^2\!\left[\eta_M\right]\mathrm{var}\!\left[\eta_{h,s}\right]$	$\ell_{h,s}$
4	$c_2^2 b_4$	$E^2\!\left[\eta_u\right]E^2\!\left[\eta_M\right]\mathrm{var}\!\left[\eta_{h,n}\right]$	$\ell_{h,n}$
5	$c_2^2 b_5$	$E^2\!\left[\eta_u\right]E^2\!\left[\eta_h\right]\mathrm{var}\!\left[\eta_{M,s}\right]$	$\ell_{M,s}$
6	$c_2^2 b_6$	$E^2\!\left[\eta_u\right]E^2\!\left[\eta_h\right]\mathrm{var}\!\left[\eta_{M,n}\right]$	$\ell_{M,n}$
7	$c_2^2 b_7$	$E^2\!\left[\eta_u\right]\mathrm{var}\!\left[\eta_{h,s}\right]\mathrm{var}\!\left[\eta_{M,s}\right]$	$\dfrac{1}{1/\ell_{h,s}+1/\ell_{M,s}}$
8	$c_2^2 b_8$	$E^2\!\left[\eta_u\right]\mathrm{var}\!\left[\eta_{h,s}\right]\mathrm{var}\!\left[\eta_{M,n}\right]$	$\dfrac{1}{1/\ell_{h,s}+1/\ell_{M,n}}$
9	$c_2^2 b_9$	$E^2\!\left[\eta_u\right]\mathrm{var}\!\left[\eta_{h,n}\right]\mathrm{var}\!\left[\eta_{M,s}\right]$	$\dfrac{1}{1/\ell_{h,n}+1/\ell_{M,s}}$
10	$c_2^2 b_{10}$	$E^2\!\left[\eta_u\right]\mathrm{var}\!\left[\eta_{h,n}\right]\mathrm{var}\!\left[\eta_{M,n}\right]$	$\dfrac{1}{1/\ell_{h,n}+1/\ell_{M,n}}$
11	$c_2^2 b_{11}$	$E^2\!\left[\eta_h\right]\mathrm{var}\!\left[\eta_{u,s}\right]\mathrm{var}\!\left[\eta_{M,s}\right]$	$\dfrac{1}{1/\ell_{u,s}+1/\ell_{M,s}}$
12	$c_2^2 b_{12}$	$E^2\!\left[\eta_h\right]\mathrm{var}\!\left[\eta_{u,s}\right]\mathrm{var}\!\left[\eta_{M,n}\right]$	$\dfrac{1}{1/\ell_{u,s}+1/\ell_{M,n}}$
13	$c_2^2 b_{13}$	$E^2\!\left[\eta_h\right]\mathrm{var}\!\left[\eta_{u,n}\right]\mathrm{var}\!\left[\eta_{M,s}\right]$	$\dfrac{1}{1/\ell_{u,n}+1/\ell_{M,s}}$
14	$c_2^2 b_{14}$	$E^2\!\left[\eta_h\right]\mathrm{var}\!\left[\eta_{u,n}\right]\mathrm{var}\!\left[\eta_{M,n}\right]$	$\dfrac{1}{1/\ell_{u,n}+1/\ell_{M,n}}$
15	$c_2^2 b_{15}$	$E^2\!\left[\eta_M\right]\mathrm{var}\!\left[\eta_{u,s}\right]\mathrm{var}\!\left[\eta_{h,s}\right]$	$\dfrac{1}{1/\ell_{u,s}+1/\ell_{h,s}}$
16	$c_2^2 b_{16}$	$E^2\!\left[\eta_M\right]\mathrm{var}\!\left[\eta_{u,s}\right]\mathrm{var}\!\left[\eta_{h,n}\right]$	$\dfrac{1}{1/\ell_{u,s}+1/\ell_{h,n}}$

i	a_i	b_i	ℓ_i
17	$c_2^2 b_{17}$	$E^2[\eta_M]\,\mathrm{var}[\eta_{u,n}]\,\mathrm{var}[\eta_{h,s}]$	$\dfrac{1}{1/\ell_{u,n}+1/\ell_{h,s}}$
18	$c_2^2 b_{18}$	$E^2[\eta_M]\,\mathrm{var}[\eta_{u,n}]\,\mathrm{var}[\eta_{h,n}]$	$\dfrac{1}{1/\ell_{u,n}+1/\ell_{h,n}}$
19	$c_2^2 b_{19}$	$\mathrm{var}[\eta_{u,s}]\,\mathrm{var}[\eta_{h,s}]\,\mathrm{var}[\eta_{M,s}]$	$\dfrac{1}{1/\ell_{u,s}+1/\ell_{h,s}+1/\ell_{M,s}}$
20	$c_2^2 b_{20}$	$\mathrm{var}[\eta_{u,s}]\,\mathrm{var}[\eta_{h,n}]\,\mathrm{var}[\eta_{M,s}]$	$\dfrac{1}{1/\ell_{u,s}+1/\ell_{h,n}+1/\ell_{M,s}}$
21	$c_2^2 b_{21}$	$\mathrm{var}[\eta_{u,s}]\,\mathrm{var}[\eta_{h,s}]\,\mathrm{var}[\eta_{M,n}]$	$\dfrac{1}{1/\ell_{u,s}+1/\ell_{h,s}+1/\ell_{M,n}}$
22	$c_2^2 b_{22}$	$\mathrm{var}[\eta_{u,s}]\,\mathrm{var}[\eta_{h,n}]\,\mathrm{var}[\eta_{M,n}]$	$\dfrac{1}{1/\ell_{u,s}+1/\ell_{h,n}+1/\ell_{M,n}}$
23	$c_2^2 b_{23}$	$\mathrm{var}[\eta_{u,n}]\,\mathrm{var}[\eta_{h,s}]\,\mathrm{var}[\eta_{M,s}]$	$\dfrac{1}{1/\ell_{u,n}+1/\ell_{h,s}+1/\ell_{M,s}}$
24	$c_2^2 b_{24}$	$\mathrm{var}[\eta_{u,n}]\,\mathrm{var}[\eta_{h,n}]\,\mathrm{var}[\eta_{M,s}]$	$\dfrac{1}{1/\ell_{u,n}+1/\ell_{h,n}+1/\ell_{M,s}}$
25	$c_2^2 b_{25}$	$\mathrm{var}[\eta_{u,n}]\,\mathrm{var}[\eta_{h,s}]\,\mathrm{var}[\eta_{M,n}]$	$\dfrac{1}{1/\ell_{u,n}+1/\ell_{h,s}+1/\ell_{M,n}}$
26	$c_2^2 b_{26}$	$\mathrm{var}[\eta_{u,n}]\,\mathrm{var}[\eta_{h,n}]\,\mathrm{var}[\eta_{M,n}]$	$\dfrac{1}{1/\ell_{u,n}+1/\ell_{h,n}+1/\ell_{M,n}}$

www.ski.se